Topography of corticopontine projections is controlled by postmitotic expression of the area-mapping gene Nr2f1

Chiara Tocco[1]*, Martin Øvsthus[2]*, Jan G. Bjaalie[2], Trygve B. Leergaard[2#], Michèle Studer[1#]

[1]*Université Côte d'Azur, CNRS, Inserm, iBV, France*

[2]*Institute of Basic Medical Sciences, University of Oslo, Oslo, Norway*

*These authors have contributed equally to the study.

#Co-last authors.

[@]Corresponding author:

Michèle Studer
iBV - Institut de Biologie Valrose
Univ. Côte d'Azur
Centre de Biochimie ; UFR Sciences
Parc Valrose, 28 avenue Valrose
06108 Nice Cedex 2
France
Tel.: +33 489150720
e-mail: Michele.studer@unice.fr

SUMMARY

Axonal projections from layer V neurons of distinct neocortical areas are topographically organized into discrete clusters within the pontine nuclei during the establishment of voluntary movements. However, the molecular determinants controlling corticopontine connectivity are insufficiently understood. Here, we show that an intrinsic cortical genetic program driven by Nr2f1 graded expression in cortical progenitors and postmitotic neurons is directly implicated in the organization of corticopontine topographic mapping. Transgenic mice lacking cortical expression of *Nr2f1* and exhibiting areal organization defects were used as model systems to investigate the arrangement of corticopontine projections. Combining three-dimensional digital brain atlas tools, *Cre*-dependent mouse lines, and axonal tracing, we show that *Nr2f1* expression in postmitotic neurons spatially and temporally controls somatosensory topographic projections, whereas expression in progenitor cells influences the ratio between corticopontine and corticospinal fibers passing the pontine nuclei. We conclude that cortical gradients of area patterning genes are directly implicated in the establishment of a topographic somatotopic mapping from the cortex onto pontine nuclei.

Keywords: corticopontine topography, layer V neurons, area mapping genes, Nr2f1, mouse models, *Thy1*-e*YFP-H* reporter line, pontine nuclei, 3D data points, interactive 3D viewer tools, anterograde fluorescent tracing

INTRODUCTION

Neuronal populations responsible for fine motor coordination are arranged in topographically organized maps in the neocortex and cerebellum exemplified by different body parts being represented in largely continuous maps in the somatosensory cortex (Chapin and Lin, 1984, Fabri and Burton, 1991, Welker, 1971, Woolsey and Van der Loos, 1970), and discontinuous, fractured maps in the cerebellum (Bower et al., 1981, Bower, 2011, Leergaard et al., 2006, Bower and Kassel, 1990, Nitschke et al., 1996, Shambes et al., 1978). The intercalated regions of this network, including the pontine nuclei, deep cerebellar nuclei, and the thalamus, receive and integrate signals ultimately resulting in coordinated and seamlessly executed behaviors (Peterburs and Desmond, 2016, Buckner, 2013, Stoodley and Schmahmann, 2010), including fine voluntary movements (Badura et al., 2013, Mottolese et al., 2013).

The pontine nuclei constitute the major synaptic relay for cerebro-cerebellar signals (Brodal and Bjaalie, 1992, Lemon, 2008, Mihailoff et al., 1985). Axonal projections originating from layer V pyramidal neurons across the neocortex are distributed in topographically organized clusters within the pontine nuclei, as shown in monkey (Brodal, 1978, Schmahmann and Pandya, 1997), cat (Bjaalie and Brodal, 1997), rat (Leergaard et al., 2000a, Leergaard et al., 2000b), and to some extent also in mice (Henschke and Pakan, 2020, Inoue et al., 1991, Proville et al., 2014). Within the pontine nuclei, the three-dimensional (3D) arrangement of clustered terminal fields, well described in rats, both preserves the overall topographical relationships of the cortical maps, but also partially overlap and introduce new spatial proximities among projections from different cortical areas (Leergaard, 2003, Leergaard and Bjaalie, 2007, Bjaalie and Brodal, 1989).

To date, the mechanisms responsible for establishing the topographic map between the neocortex and pontine nuclei are poorly understood. The leading proposition, referred to as chrono-architectonic hypothesis, postulates that the complex 3D topography is a product of straightforward spatio-temporal gradients, possibly combined with non-specific chemo-attractive mechanisms (Altman and Bayer, 1996, Leergaard, 2003, Leergaard and Bjaalie, 2007, Leergaard et al., 1995). Recent new discoveries open the possibility that other mechanisms are also in action during the establishment of the corticopontine maps. Several lines of evidence point to a functional role of gradients in gene expression during topography

72 of sensory maps in several systems (D'Elia and Dasen, 2018, Erzurumlu et al., 2010, Fritzsch
73 et al., 2019, McLaughlin and O'Leary, 2005), but whether this process is also operative during
74 establishment of corticopontine topography is not completely understood. A recent study has
75 shown that postmitotic graded expression of the HOX gene *Hoxa5* is directly involved in
76 imparting an anterior to posterior identity to pontine neurons, (Maheshwari et al., 2020),
77 suggesting that pontine nuclei could play an instructive and attractive role in establishing
78 corticopontine topographical organization. Whether expression in gradients of molecular
79 factors along the antero-posterior (AP) or medio-lateral (ML) axes of the cerebral cortex also
80 contributes to determine the topography of corticopontine projections is still not known.
81 Layer V neurons from the anterolateral cerebral cortex project to the central regions of the
82 pontine nuclei, while more medially located cortical regions project to more external parts;
83 projections from motor areas are distributed more medially and rostrally, with projections
84 from somatosensory areas reaching the middle and caudal parts of the pontine nuclei. Finally,
85 auditory and visual cortical projections innervate the dorsolateral regions of the pontine
86 nuclei (Leergaard et al., 2004, Leergaard and Bjaalie, 2007). The fine-tuned and precise
87 topography between the cortex and pontine nuclei leaves open the possibility for cortical
88 neurons being intrinsically programmed to target specific groups of pontine neurons, possibly
89 coupling intrinsic (cell-type specification) and extrinsic (chemo-attractive) mechanisms in
90 directing proper topographical innervation to the pontine nuclei.

91 Area mapping genes are expressed in gradients along the different axes of the cortical
92 primordium and known to modulate the size and position of future cortical areas (Alfano and
93 Studer, 2012, Cadwell et al., 2019, O'Leary and Sahara, 2008). These genes are therefore good
94 candidates for modulating topographic mapping. In mice, the Nr2f1 gradient expression
95 appears to be a particularly strong candidate for having a formative role during the
96 establishment of topographic maps (Armentano et al., 2007, Zhou et al., 2001, Liu et al.,
97 2000). For instance, Nr2f1 (also known as COUP-TFI) is expressed in cortical progenitor cells
98 from embryonic day E9.0 in a high caudo-lateral to low rostro-medial gradient fashion, and
99 the gradient expression is maintained in postmitotic descendants as well as postnatally when
100 the cortical area map is completed (Bertacchi et al., 2019, Flore et al., 2017, Tomassy et al.,
101 2010). We thus hypothesized that Nr2f1 could represent one of these factors able to control
102 topographic corticopontine mapping during corticogenesis.

103 To test this hypothesis, we made use of cortico-specific *Nr2f1* conditional knockout mice as
104 an i*n vivo* model system and a paradigm to investigate the contribution of cortical genetic
105 programs in the establishment of topographic corticopontine projections. Two distinct
106 conditional mouse lines, in which *Nr2f1* is knocked out in either cortical progenitor cells or
107 postmitotic cortical neurons (Alfano et al., 2014, Armentano et al., 2007) were crossed to the
108 *Thy1*-e*YFP-H* reporter line (Feng et al., 2000), in which YFP is highly expressed in cortical layer
109 V pyramidal neurons and their axonal projections (Porrero et al., 2010). The distribution of
110 fluorescent YFP signals as well as anterogradely labelled corticopontine projections were
111 evaluated by side-by-side comparison of spatially corresponding microscopic images of
112 conditional knock-out and control animals, and by 3D visualization of extracted point-
113 coordinated data representing labelling. Our data indicate that cortical Nr2f1 expression plays
114 a dual role in controlling the spatio-temporal development of corticopontine projections.
115 While early expression in progenitor cells influences the ratio between corticofugal fibers
116 passing the pontine nuclei, thus precluding any topographic function, loss of solely
117 postmitotic late expression specifically affects topographic pontine mapping. Overall, our
118 results demonstrate that intrinsic genetic programs and postmitotic graded expression of
119 cortical area mapping genes are implicated in the spatio-temporal establishment of area-
120 specific targeting of corticopontine neurons.

121 **RESULTS**

122 **Benchmark 3D topographic organization of corticopontine projections in wild-type mice**

123 To first establish a 3D reference of the topographical organization of corticopontine
124 projections in normal adult mice, we used tract tracing data from the *Allen Institute Mouse*
125 *Brain Connectivity Atlas* (Wang et al., 2020) to visualize the spatial distribution of the pontine
126 projections of motor and somatosensory neocortical areas. **Figure 1** shows a flowchart of the
127 different processing and analytic steps used for the different animal groups. Before evaluating
128 the YFP signal in the cortex, pontine nuclei, and medulla oblongata of *Nr2f1* mutant mice, we
129 first determined the normal topographical organization of motor and somatosensory
130 corticopontine projections in wild-type mice. We semi-quantitatively recorded anterogradely

131 labelled corticopontine projections from microscopic images as 3D data points that were co-
132 visualized in a 3D viewer tool (**Figure 2**).
133 3D visualization of data points representing corticopontine labelling arising from two similarly
134 located tracer injections in the S1 face representation in C57BL/6J wild-type mice from the
135 *Allen Mouse Brain Connectivity* (**Figure 2A-E**), and our control mice (**Figure 2F-J**), showed
136 similar distributions of labelling in the central core of the pontine nuclei, resembling the
137 distribution of corticopontine projections from the somatosensory face region reported
138 earlier in rats (Leergaard et al., 2000b). Comparison of data points representing
139 corticopontine projections from different locations across the primary/secondary motor
140 cortex (M1, M2; n = 6) and primary somatosensory cortex (S1; n = 5) in wild type mice, showed
141 that motor and somatosensory corticopontine projections target largely segregated
142 subspaces of the pontine nuclei, with somatosensory projections located predominantly in
143 central and caudal parts, while projections originating from the motor cortex were located
144 more rostrally and ventrally, partly surrounding the sensory projections externally (**Figure 3A-**
145 **G**).

146

147

148 ***Figure 1. Experimental and analytic workflow.*** *The three columns represent workflow steps, with logic and*
149 *outputs, followed to investigate topographical organization in the different experimental paradigms. (**A**)*
150 *The left column represents the workflow for generating a 3D control topographic map of corticopontine*
151 *projections using public tract tracing data (https://connectivity.brain-map.org/), mapped and compared in*
152 *a 3D reference atlas space. (**B**) The middle and right column represent the two paradigms investigated in*
153 *conditional mouse models, with the analytic steps performed in adult control, Emx1-cKO and Nex-cKO*
154 *mutant animals (middle column, paradigm 1), and the tract tracing study of the 3D topography of motor*
155 *and somatosensory corticopontine projections in young control and Nex-cKO mutant animals (right column,*
156 *paradigm 2). All images were spatially registered to the Allen mouse brain atlas (CCFv3; Wang et al., 2020)*
157 *prior to analyses, to facilitate comparison of images and spatial distribution patterns. Results are shown in*
158 *Figures 2-7.*

159

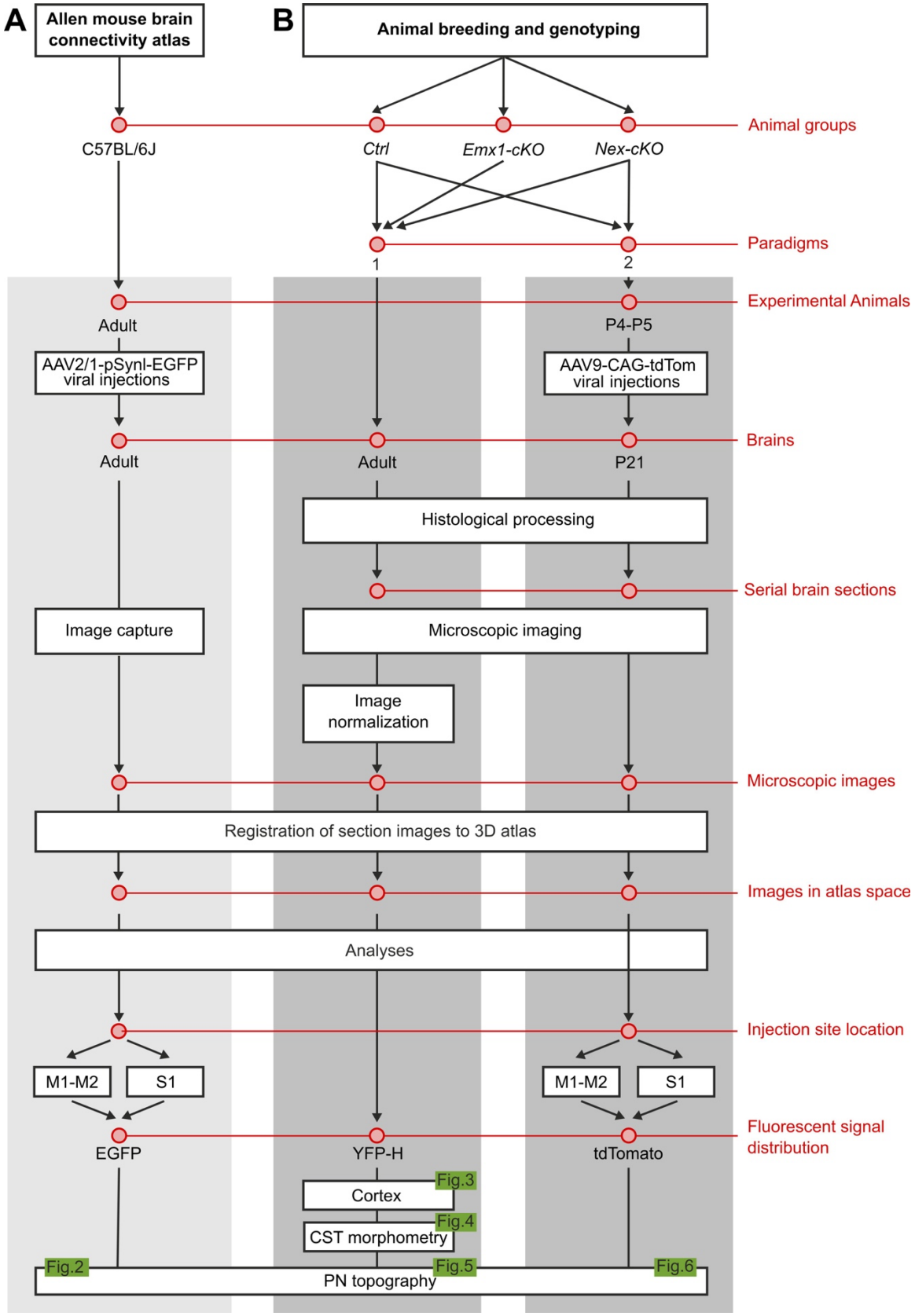
A
Allen mouse brain connectivity atlas
B
Animal breeding and genotyping
Animal groups
C57BL/6J
Ctrl
Emx1-cKO
Nex-cKO
Paradigms
1
2
Experimental Animals
Adult
P4-P5
AAV2/1-pSynI-EGFP viral injections
AAV9-CAG-tdTom viral injections
Brains
Adult
Adult
P21
Histological processing
Serial brain sections
Image capture
Microscopic imaging
Image normalization
Microscopic images
Registration of section images to 3D atlas
Images in atlas space
Analyses
Injection site location
M1-M2
S1
M1-M2
S1
Fluorescent signal distribution
EGFP
YFP-H
tdTomato
Fig.3
Cortex
Fig.4
CST morphometry
Fig.2
Fig.5
Fig.6
PN topography

160

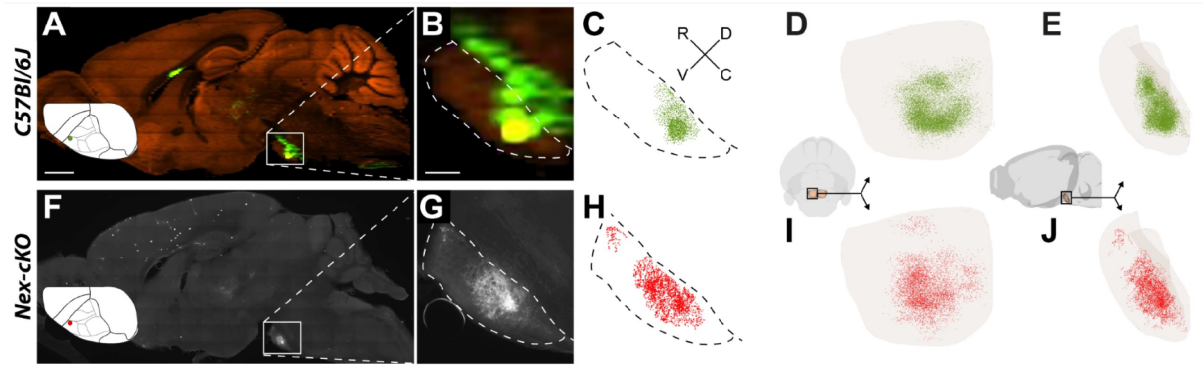

Figure 2. Semi-quantitative recording and 3D visualization of corticopontine tracing data. *Examples illustrating the data acquisition of corticopontine projections labelled by viral tracer injection in the S1 face representation in C57BL/6J mice from the Allen Mouse Brain Connectivity Atlas (**A-E**), and control mice from the present study (**F-J**). Panels **A,B** and **F,G** show anterogradely labelled axons observed by fluorescence microscopy in two sagittal sections through the right pontine nuclei. **C** and **H** indicate semi-quantitatively recorded point corresponding to the observed density of labelling observed in **B** and **G**. Panels **D,E** and **I,J** show the 3D point populations recorded in each case together with a transparent surface rendering of the right pontine nuclei, seen from ventral (**D,I**) and medial (**E,J**) views, as indicated in the 3D inset. In both cases, the S1 corticopontine projections are distributed in dense clusters located centrally in the pontine nuclei. Abbreviations: C, caudal; D, dorsal, R, rostral, V, ventral. Scale bars, 1 mm (**A,B**) and 200 µm (**B,G**).*

To further test whether motor and somatosensory corticopontine projections follow the topographical distribution principles as described in rats (Leergaard and Bjaalie, 2007), we selected experiments with tracer injections located progressively more medially and caudally in the cerebral cortex (**Figure 3H)**, following the cortical neurogenetic gradient that ripples out from the anterolateral cortex (Smart, 1984, Leergaard and Bjaalie, 2007). The 3D visualizations shows that mouse corticopontine projections are concentrically organized, with projections from the anterolateral neocortex located centrally in the pontine nuclei, and projections from more medially located parts of somatosensory and motor cortex distributed in progressively more peripheral parts of the pontine nuclei, and attaining a circular shape surrounding the central core (**Figure 3I-N**), in agreement with topographical distribution principles shown in rats (Leergaard and Bjaalie, 2007). Taken together, our findings confirm that the somatosensory and motor neurons of the mouse cortex project to largely separate parts of the pontine nuclei (Henschke and Pakan, 2020, Inoue et al., 1991, Proville et al., 2014), with clustered terminal fields that are topographically distributed in the same concentric fashion as previously shown in rats (Leergaard et al., 2000a, Leergaard and Bjaalie, 2007). The 3D point data presented here are also used below as supplementary control data,

and as benchmarks for interpreting YFP expression and tract-tracing results in *Nr2f1* mutant mice.

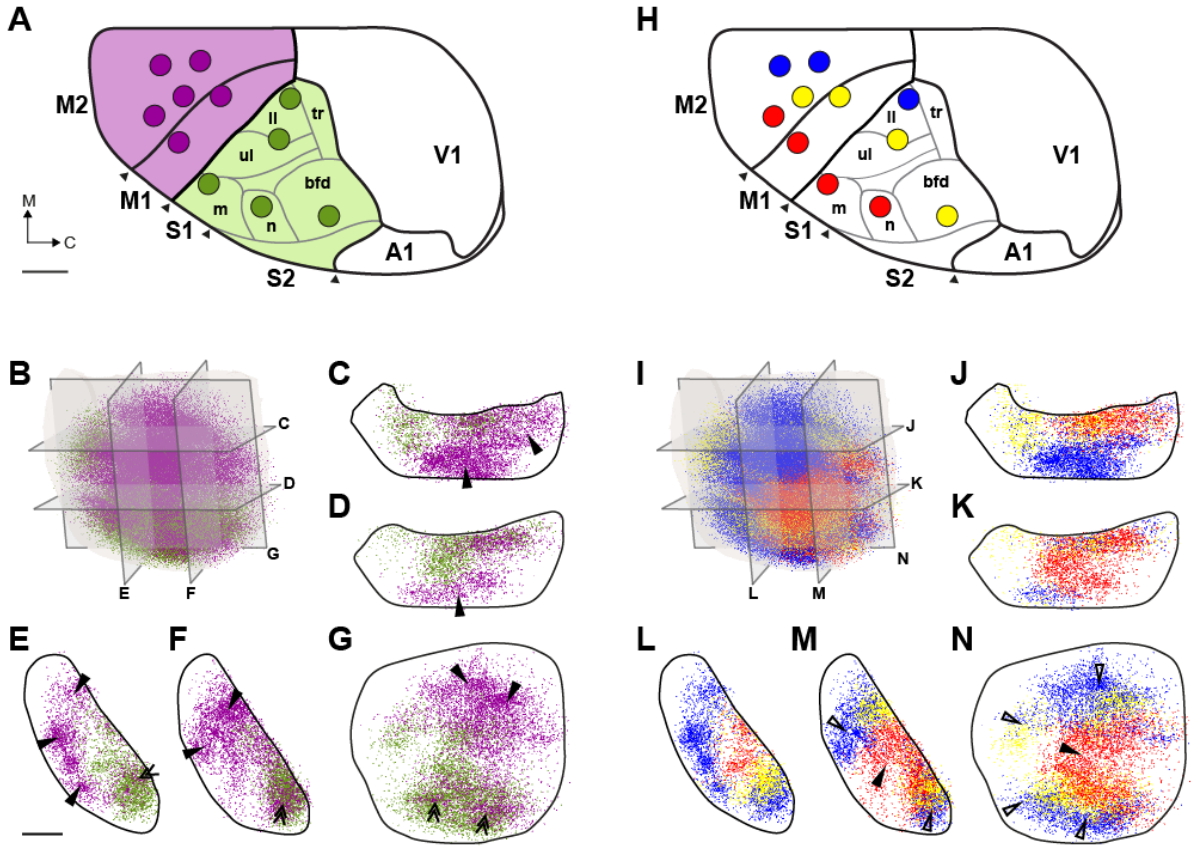

Figure 3. Topographical organization of corticopontine projections in wild-type mice. *3D visualizations of point clouds representing spatial distribution of anterogradely labeled corticopontine axons in wild-type mice from the Allen Mouse Brain Connectivity Atlas, injected with the anterograde tracer EGFP in the primary (M1)/secondary (M2) motor cortex or primary somatosensory (S1) cortex, at locations indicated with color coded circles in* ***A*** *and* ***H****. (****B, I****) 3D visualizations of axonal labelling semi-quantitatively represented by points, inside a surface rendering of the outer boundaries of the right pontine nuclei (transparent grey surface) shown ventrally. A grid of transparent grey planes with sagittal, transversal, and frontal orientation, relative to the pontine nuclei, indicate the position and orientation of ~100 µm thick digital slices cut through the point clouds, shown in* ***C-G****, and* ***J-N****. (****B-G****) 3D co-visualization of all data points representing corticopontine projections from the 11 cases, with purple points representing projections from M1/M2, and green points representing projections from S1. The slices through the point clouds show that motor and somatosensory areas largely target different parts of the pontine nuclei, with projections from M1 and M2 located more peripherally towards rostral, ventral, and medial than projections from S1 (arrowheads in* ***C-G****), but also that motor and sensory projections overlap caudally in the pontine nuclei (double arrowheads in* ***E-G****). (****I-N****) 3D co-visualization of all data points from the 11 cases, color coded in red, yellow or blue according to the location of the cortical injection sites from anterolateral (red) progressively towards medial or posterior (yellow, blue). The slices through the point clouds reveal a concentric arrangement in the pontine nuclei, with projections from the anterolateral parts of the M1/M2 and S1 located centrally and medially (arrowheads in* ***M, N****), and projections from more medial and posterior cortical locations progressively shifted towards rostral, caudal, and lateral (unfilled arrowheads in (****M,N****). Abbreviations: A1, primary auditory cortex; bfd, barrel field; ll, lower limb; m, mouth; M1, primary motor cortex; M2, secondary motor cortex; n, nose; S1, primary somatosensory cortex; S2, secondary somatosensory cortex, tr, trunk; ul, upper limb. Scale bars, 1 mm (****A,H****), 200 µm (****B-G, I-N****).*

216 **Different area-specific layer V neuron distribution in cortices lacking Nr2f1**

217 To assess the influence of cortical area mapping on the establishment of topographical
218 organization in mouse corticopontine projections, we used as experimental model systems
219 *Nr2f1* deficient mice (Alfano et al., 2014, Armentano et al., 2007), and first investigated the
220 spatial organization of layer V cortical distribution and corticopontine axonal projections in
221 mutant adults compared to control animals. To this purpose, we used two well-established
222 conditional *Nr2f1* mouse mutants: the *Nr2f1*$^{fl/fl}$*::Emx1-Cre* mouse, in which *Nr2f1* expression
223 is abolished from early cortical progenitor cells at mouse embryonic (E) age 9.5 (Armentano
224 et al., 2007), and the *Nr2f1*$^{fl/fl}$*::Nex-Cre* mouse in which *Nr2f1* expression is inactivated at later
225 stages (E11.5-E12), solely in cortical postmitotic neurons (Alfano et al., 2014, Goebbels et al.,
226 2006). Both mouse lines were crossed to the *Thy1-eYFP-H* reporter line to specifically restrict
227 signal expression to the majority of layer V pyramidal neurons, allowing labelling of
228 subcortical projection neurons, including corticospinal and corticopontine fibers (Harb et al.,
229 2016, Porrero et al., 2010). For simplicity, both lines will be named from here on *Emx1-cKO*
230 and *Nex-cKO*, respectively.

231 In agreement with the earlier detailed report by Porrero et al. (Porrero et al., 2010), we
232 observed substantial YFP signal expression in the hippocampus, tectum, and pontine nuclei,
233 as well as in the globus pallidus, claustrum, endopiriform nucleus, nucleus of the lateral
234 olfactory tract, mammillary nuclei, piriform area, and the substantia innominata in adult mice
235 (**Figure 4A**). Signal expression was also seen in the vestibular nuclei, deep cerebellar nuclei,
236 and cerebellum. Although signal expression was present in almost the same regions in 2-
237 months-old mutant mice as in controls, more detailed analysis of signal expression in
238 neocortical areas revealed some distinct differences in the spatial distribution of *Emx-cKO* and
239 *Nex-cKO* brains relative to their respective controls, and between the two conditional lines.
240 We used a semi-quantitative scoring system to estimate the amount of signal expression
241 across the cerebral cortex, in areas defined by delineations derived from spatially registered
242 overlay images from the *Allen Mouse Brain Atlas* ((Wang et al., 2020); **Figure 1; Figure 4B-D'**).
243 In control animals, the distribution of YFP-expressing neurons followed a rostrally high to
244 caudally low gradient (**Figure 4A, B, B'**), in line with the strong YFP signal in layer V neurons
245 of M1 and S1 areas known to contain representations of the trunk and limbs and to the earlier

246 documented high numbers of layer V neurons in the rostrally located motor areas (Polleux et
247 al., 1997, Shepherd, 2009, Porrero et al., 2010). Strong staining in these areas resulted in
248 bright signal expression in the cerebral peduncle and CST (**Figure 4A).** Notably, in the cortex
249 of mutant animals, this gradient was disrupted and the YFP signal more homogenously
250 distributed along the anteroposterior axis and at both lateral and medial levels (**Figures 4C,**
251 **C' and D, D'**). Increased YFP expression was observed caudally in the occipital and
252 retrosplenial cortex in both groups of mutant mice, in conjunction with decreased YFP signal
253 in frontal areas, which was particularly more pronounced in *Nex-cKO* than *Emx-cKO* mice
254 (**Figures 4B-F**). Interestingly, the highest signal of YFP expression was observed in the *Emx1-*
255 *cKO* S1 cortex (**Figure 4B, C, F**), but no statistical difference compared to controls was
256 detected in S1 of *Nex-cKO* brains (**Figure 4B, D, F**). Together, these data indicate a different
257 role for Nr2f1 in early progenitor cells (*Emx-cKO*) and late postmitotic neurons (*Nex-cKO*)
258 during layer V differentiation, as assessed by YFP signal expression, across all cortical areas,
259 particularly in M1 and S1 (**Figure 4F**).
260
261 ***Figure 4 – Cortical distribution of YFP-positive layer V pyramidal neurons in control, Emx1-cKO and Nex-***
262 ***cKO adult brains.*** *(**A**) Fluorescence microscopy image of a representative sagittal section from a Thy1-YFP-*
263 *H mouse brain, showing widespread YFP expression. (**B-D/B'-D'**) Fluorescence microscopy images from*
264 *sagittal sections located laterally (**B-D**) and more medially (**B'-D'**) in Ctrl, Emx1-cKO, and Nex-cKO brains,*
265 *with custom made, spatially corresponding CCFv3 atlas diagrams superimposed on the microscopic images*
266 *to define the location of different cortical areas. (**E**) Semi-quantitative scale used to score the amount of*
267 *signal expression: 0, attributed to absence of positive cells (not shown); 1, very few and sparse cells with*
268 *low to medium signal intensity; 2, moderate number of sparse cells with moderate to high signal intensity;*
269 *3, high number of partially overlapping cells with high signal intensity; 4, very high number of extensively*
270 *overlapping cells with high to very high signal intensity. (**F**) Column graphs showing the scoring of YFP-H*
271 *signal expression across cortical areas in adult Ctrl (grey), Emx1-cKO (light blue) and Nex-cKO (red) mice. In*
272 *Emx1-cKO samples, less signal expression is seen in the most anterior regions (ACC and M2, but not M1),*
273 *whereas increased signal is quantified in parietal and occipital regions (S1, A, V. and RSC), relative to the*
274 *control condition. In Nex-cKO animals, the amount of signal is reduced in ACC, M2 and M1, with no*
275 *statistical difference in S1 compared to controls, but with increased amount of signal in A, V, and RSC, even*
276 *if lower than in Emx1-cKOs. * < 0.05, **< 0.01, ***<0.005, #<0.0001. Data are represented as mean ± SEM.*
277 *Data were analyzed with 2way-ANOVA test and corrected for multiple comparison with the Bonferroni test*
278 *(see also **Supplementary Table 4**). Ctrl, n=6; Emx1-cKO, n=4, Nex-cKO, n=4.. Abbreviations: A, auditory*
279 *cortex; ACC, anterior cingulate cortex; CA1, cornu ammonis area 1; CB, cerebellum; CP, cerebral peduncle;*
280 *CST, corticospinal tract; Cx, cortex; fi, fimbria; GC, gustatory cortex; LFP, longitudinal fascicle of the pons;*
281 *M1, primary motor cortex; M2, secondary motor cortex; MB, mammillary body; OB, olfactory bulb; PFC,*
282 *prefrontal cortex; PN, pontine nuclei; RSC, retrosplenial cortex; S1, primary somatosensory cortex; SC,*
283 *superior colliculus; Sb, subiculum; Th, thalamus; V, visual cortex. Scale bars: 1000µm (**A**); 500µm (**B-D; B'-***
284 ***D'**).*
285

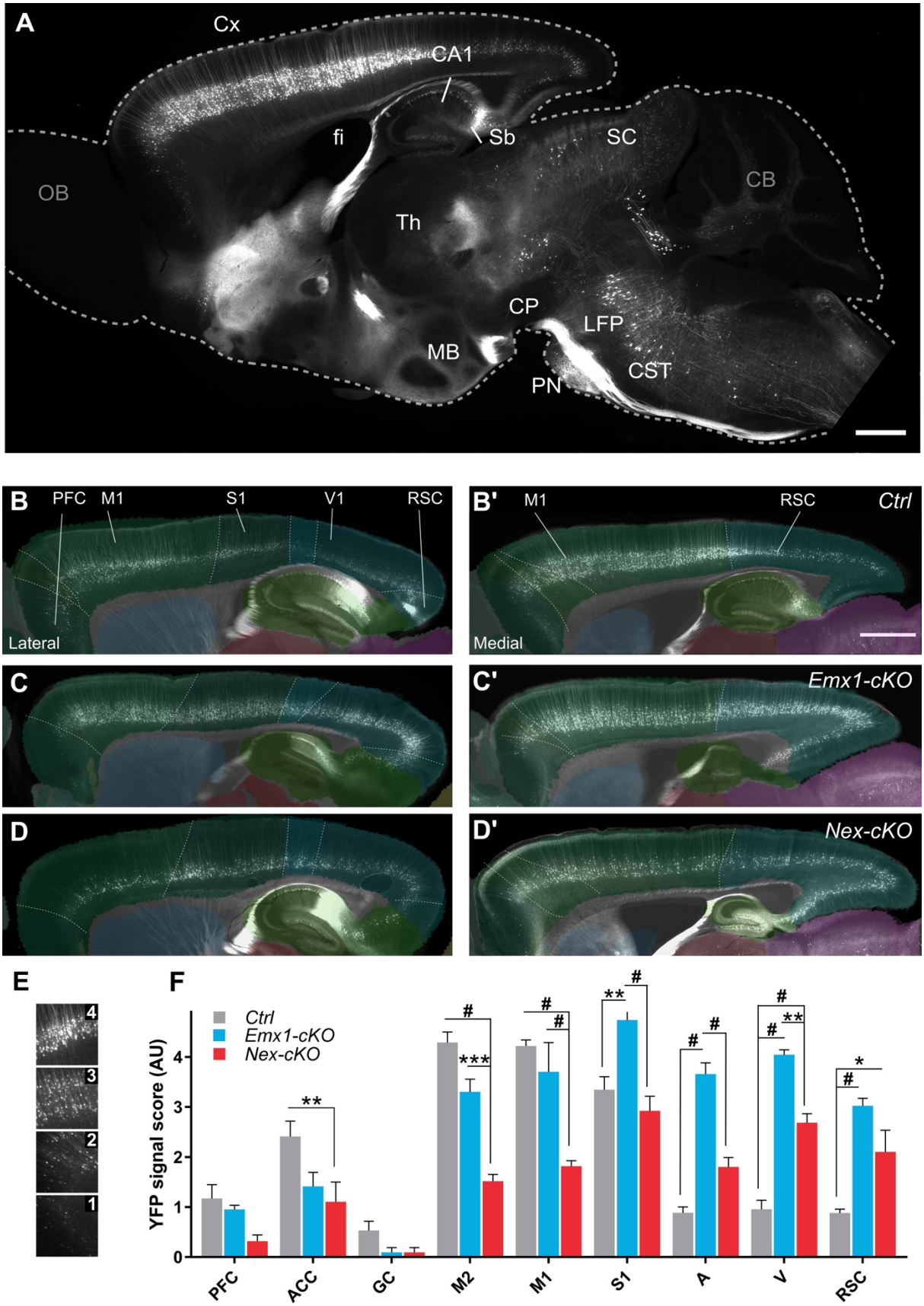
A
Cx
CA1
fi
Sb
SC
OB
CB
Th
CP
LFP
MB
CST
PN
B
PFC
M1
S1
V1
RSC
Lateral
B'
M1
RSC
Ctrl
Medial
C
C'
Emx1-cKO
D
D'
Nex-cKO
E
4
3
2
1
F
Ctrl
Emx1-cKO
Nex-cKO
YFP signal score (AU)
0
1
2
3
4
PFC
ACC
GC
M2
M1
S1
A
V
RSC

286

287 **Abnormal corticospinal projections and fasciculation in *Nr2f1* mutant brains**

288 Next, we asked whether the impaired cortical distribution of YFP expressing layer V neurons
289 in mutant mice influences the integrity of subcortical axonal projections. In all cases (mutant
290 and controls alike), strong YFP signal expression was seen bilaterally in the main corticofugal
291 pathways (**Figure 4A)**, visible as longitudinally oriented fiber bundles coursing through the
292 caudoputamen towards the cerebral peduncle (**Figure 5A-D)**, passing dorsal to the pontine
293 nuclei as the longitudinal fasciculus of the pons (**Figure 5B'-D')**, and continuing through the
294 brain stem towards the spinal cord as the CST. Since a large fraction of the corticobulbar fibers
295 terminate in the pontine nuclei (Tomasch, 1969, Tomasch, 1968), we hypothesized that
296 abnormal distribution of YFP-expressing layer V neurons observed in mutant mice (**Figure 4**)
297 might affect corticopontine innervation, and could be reflected in an abnormal size of the
298 pontine longitudinal fascicle as it enters the cerebral peduncle and exits the pons in rostral
299 and caudal positions to the pontine nuclei, respectively. To evaluate this, we measured the
300 dorsoventral width of the longitudinal fascicle of the pons in sequential sections along the
301 medio-lateral axis. The measurements were taken at rostral and caudal levels to the pontine
302 nuclei in the three genotypes (**Figure 5A'**). Surprisingly, we found the lateral part of the
303 fascicle to be wider at both rostral and caudal levels in *Nex-cKO* mice compared to *Emx1-cKO*
304 and controls, while being narrower medially (see red area chart in **Figure 5E, F**). This suggests
305 that the longitudinal fascicle of the pons is flattened and expanded laterally upon Nr2f1
306 inactivation in postmitotic neurons. Smaller differences were observed in the *Emx1-cKO*
307 fascicle which shape was however more similar to controls than to the *Nex-cKO* one (blue
308 area chart in **Figure 5E, F**). This is also supported by quantification of the total surface of the
309 longitudinal fascicle of the pons at rostral and caudal levels, which shows a significant surface
310 reduction at caudal but not rostral levels in *Emx1-cKO* mice (**Figure 5G, H**). These data indicate
311 that loss of Nr2f1 in progenitors results in fewer YFP-expressing fibers passing the pontine
312 nuclei towards the brain stem to form the CST.

313 Moreover, we observed, caudal to the pontine nuclei, abnormally widespread fiber fascicles
314 in the CST of mutant animals (arrowheads in **Figure 5C', D'**). To determine whether this was
315 a significant difference between animal groups, we estimated the degree of fiber bundle
316 fasciculation in the CST of *Emx1-cKO* and *Nex-cKO* mice. At locations of 250μm and 500μm

317 caudal to the pontine nuclei (**Figure 5A'**), we measured the total dorsoventral width of the
318 CST at several mediolateral levels and subtracted the width of gaps between the YFP-
319 expressing fiber bundles at the same levels. The ratio of the total width of the CST and width
320 of the fibers only was used as a measure of the fasciculation index **(Figure 5I**). Notably, in both
321 groups of mutant mice we found a lower degree of fasciculation in the CST which was more
322 pronounced at the most caudal level (**Figure 5I**). Together, these data show that *Nr2f1*
323 expression (both in cortical progenitor cells and postmitotic cells) controls the diameter,
324 shape and degree of fasciculation of the CST originating from layer V neurons.

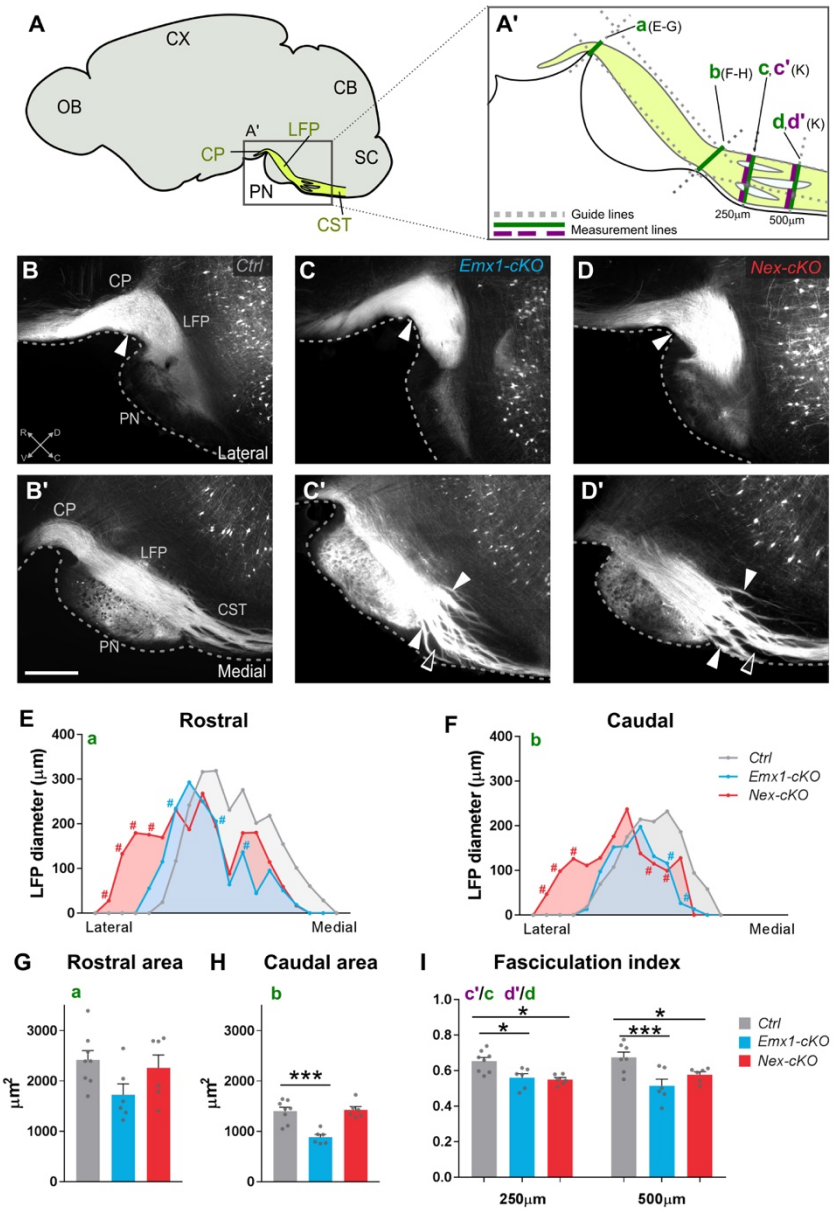

325

326 ***Figure 5 – Loss of Nr2f1 function leads to abnormal corticospinal projections and fasciculation.*** *(A)*
327 *Schematic diagram of a sagittal mouse brain section showing the location of the pontine nuclei (PN) and*

*descending fiber tracts (yellow) in the cerebral peduncle (CP), longitudinal fascicle of the pons (LFP) and corticospinal tract (CST) at level of the pons. (**A'**) Diagram taken from A illustrating the different measurements shown in E-I. The frame reflects the region shown in **B-D** and **B'-D'** in control (Ctrl), Emx1-cKO and Nex-cKO animals. (**B-D**) Lateral sagittal section showing the corticospinal tract entering the pons level as a continuation of the cerebral peduncle. White arrowheads point to the site of measurement plotted in E, showing a similar thickness of the bundle in the three genotypes. (**B'-D'**) Medial sagittal section showing the corticospinal tract passing dorsal to the pontine nuclei and defasciculating prior to entering the spinal cord. Full arrowheads point to fiber bundles (thinner and more dispersed in both Emx1-cKO and Nex-cKO mutants), empty arrowheads point to empty spaces between bundles. (**E, F**) Plots showing LFP diameter measurements obtained from lateral to medial before and after innervating the pontine nuclei (rostral and caudal respectively) for the three genotypes. Each measurement represents the average value of corresponding sections among distinct animals and each position on the x-axis represents a specific section of the series. (**G-H**) Column graphs showing average values of the area under the curves in **E-F**. A comparable number of fibers reach the cerebral peduncle in the three genotypes (**G**). In Emx1-cKO brains fewer fibers are seen to exit the level of the pons compared to control- and Nex-cKO brains (**H**). (**I**) Column graph showing CST fasciculation index, based on measurements of total thickness and fiber thickness (green and purple line respectively in **A'**) performed at 250 and 500 µm from the terminal edge of the pontine nuclei. A ratio between the two measurements was calculated for each position. Data are represented as mean ± SEM. Data were analyzed with 2way-ANOVA test (**E-F**) or ordinary one-way ANOVA test (**G-I**) and corrected for multiple comparison with the Bonferroni test (see also Supplementary Table 4). Ctrl, n=8; Emx1-cKO, n=6; Nex-cKO, n=6. #<0.05 (**E-F**) * < 0.05, **< 0.01, ***<0.005 (**G-I**). Abbreviations: CB, cerebellum; CP, cerebral peduncle; CST, corticospinal tract; CX, cortex; LFP, longitudinal fascicle of the pons; OB, olfactory bulb; PN, pontine nuclei; SC, spinal cord. Scale bar=500µm.*

Dual role of Nr2f1 in targeting corticopontine projections

To evaluate whether topographical organization of corticopontine projections was dependent on proper cortical area mapping, we assessed the spatial distribution of YFP signal expression within the pontine nuclei by comparing intensity-normalized microscopic images of spatially corresponding sagittal sections from the brains of *Emx-cKO*, *Nex-cKO* and control animals (**Figure 6A**). In all mice, widespread signal expression was seen across most parts of the pontine nuclei (**Figure 6B-L**). A complete documentation of spatially comparable images showing YFP expression in the pontine nuclei of all mutant mice and controls is provided in **Supplementary Figures 1 and 2**. In control brains, we observed a strong YFP signal in central parts of the pontine nuclei, with the densest expression tending to surround a centrally located zone exhibiting less dense signals (**Figure 6B-E**). This region of the pontine nuclei typically receives strong projections from S1 areas (**Figure 3**). Some signal expression was also visible in medial parts of the pontine nuclei (**Figure 6D, E**), which is known to receive projections from the cortical motor areas (**Figure 3**). By contrast, signal expression was lower

366 in rostral and lateral parts of the pontine nuclei (**Figure 6B, C, E**), which are known to receive
367 projections from visual and auditory areas of the cerebral cortex (Inoue et al., 1991, Leergaard
368 and Bjaalie, 2007).

369 Interestingly, *Emx-cKO* mice showed a relatively homogeneous signal distribution across all
370 parts of the pontine nuclei, and notably also displayed more signal expression in the
371 dorsolateral regions (**Figure 6F-I**). Signal expression was also present in the medial part of the
372 nuclei, albeit with lower density than in the central region (**Figure 6G-I**). This observation fits
373 well with the finding of more extensive YFP signal expression in the occipital cortex (**Figure**
374 **4C,C'**), which projects to the dorsolateral pontine nuclei. By comparison, the signal expression
375 observed in *Nex-cKO* animals was more constrained and predominated in rostrally and
376 caudally located clusters extending from the cerebral peduncle towards the ventral surface
377 of the pons, and medially surrounding a central core in which little signal was expressed
378 (**Figure 6J-M**). These clusters were more peripherally located than the clustered signal
379 expression observed in control animals (**Figure 6J-M**). Notably, in all *Nex-cKO* cases little signal
380 expression was seen in the central region of the PN (unfilled arrowheads in **Figure 6J-L**),
381 despite the presence of YFP-expressing layer V neurons in S1 (**Figure 4D,D, F**). This central
382 region is normally innervated by projections from the face representations located in S1
383 (**Figures 2, 3**).

384 Taken together, these findings show that corticopontine projections are abnormally
385 distributed in *Nr2f1* cortical deficient mice, with more homogenously (non-specifically)
386 distributed expression in *Emx1-cKO* mice, and more peripherally distributed signal expression
387 in *Nex-cKO* mice, that display reduced expression in the central region of the pontine nuclei
388 normally receiving S1 projections. In both mutant groups the signal expression was expanded
389 to dorsolateral regions of the pontine nuclei that normally are innervated by projections from
390 occipital cortical areas. This suggests that cortical Nr2f1 graded expression in postmitotic
391 neurons is directly involved in the establishment of topographically organized corticopontine
392 projections.

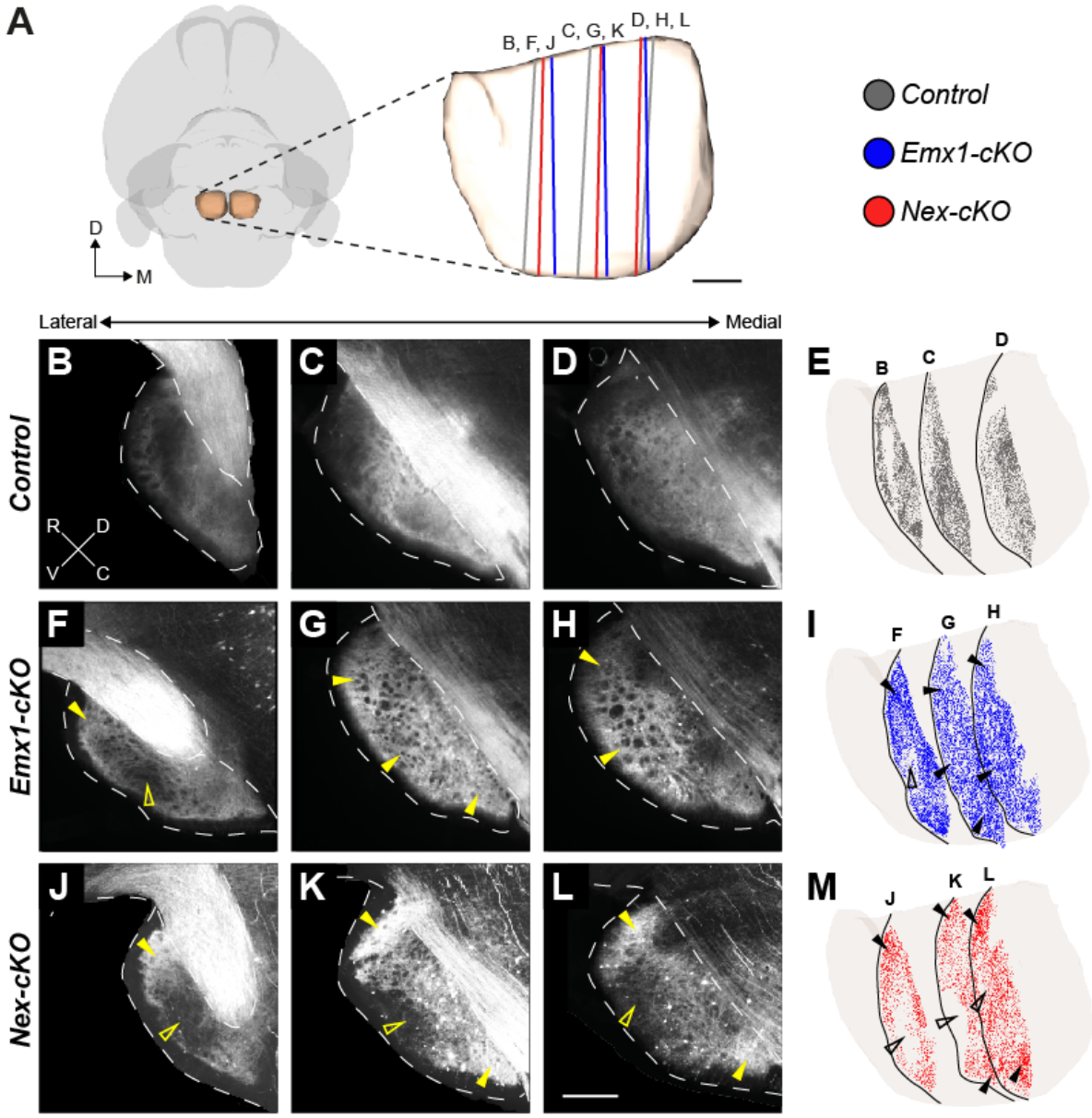

Figure 6. Distribution of YFP signal expression in the pontine nuclei in knock-out mice and controls. *(**A**) 3D representation of the outer surfaces of the brain (transparent grey) and pontine nuclei (transparent brown) from the Allen mouse brain atlas. Pontine nuclei enlarged in ventral view with colored lines representing the location and orientation of the sagittal sections shown in **B-M**. (**B-D, F-H, J-L**) Fluorescence microscopy images of sagittal sections from corresponding mediolateral levels of the pontine nuclei, showing the spatial distribution of YFP signal expression in control, Emx1-cKO, and Nex-cKO mice, respectively. (**E, I, M**) 3D visualization of the transparent external surface of the pontine nuclei in an oblique view from ventromedial, with point coded representations of signal expression from the sagittal sections shown in **B-D**, **F-H**, and **J-L**, respectively. Filled yellow or black arrowheads point to regions with increased signal expression in mutant mice, while non-filled arrowheads indicate regions with decreased signal expression. In control mice (**B-E**), signal expression is primarily seen in central and caudal parts of the pontine nuclei, while in Emx1-cKO mice (**F-I**) signal expression is more widespread and diffuse throughout the entire pontine nuclei, including more peripheral parts of the pontine nuclei towards rostral, ventral and caudal positions (filled arrowheads in G-I). In Nex-cKO mice (**J-M**), signal expression is reduced in the central core region of the pontine nuclei (non-filled arrowheads in **K-M**), while being increased in peripheral (rostral and caudal) regions of the pontine nuclei. Abbreviations: C, caudal; D, dorsal; M, medial, PN, pontine nuclei; R, rostral. Scale bars, 200 µm.*

411 **Altered somatosensory topographic projections in *Nex-cKO* adult mutant mice**

412 In addition to Nr2f1 gradient expression in cortical progenitors and early postmitotic neurons,
413 high expression in primary sensory areas, in which different sensory surfaces are
414 topographically organized, is maintained at postnatal stages and still consistent with a high
415 caudolateral to low anteromedial gradient (**Figure 7A**). To further and directly support our
416 hypothesis of a cortical influence in topographical pontine mapping, we injected the AAV9-
417 CAGtdTomato anterograde viral tracer (Pourchet et al., 2021) in motor, lateral or medial S1
418 cortex of 5 days-old (P5) *Nex-cKO* mice and littermate controls (**Figure 7B**). The mice were
419 sacrificed at P21 and brain sections analyzed microscopically. All histological sections were
420 spatially registered to the *Allen Mouse Brain Atlas* (common coordinate framework, CCF3;
421 (Wang et al., 2020)), and the location of tracer injections sites were mapped in the same atlas
422 space (**Figure 7B**). For each injection site location in a *Nex-cKO* brain, we selected either the
423 most corresponding control experiment or wild-type tract-tracing data from the *Allen Mouse*
424 *Brain Connectivity Atlas* (**Figures 2A-E and 3**), as additional controls.

425 In all control mice, the spatial distributions of corticopontine projections (dark gray point
426 clouds in **Figure 7**) were comparable with the labelling patterns seen in corresponding wild-
427 type tracing data from the *Allen Mouse Brain Connectivity Atlas*. As expected, tracer injections
428 into motor areas gave rise to labelled axonal clusters located rostrally, caudally, and medially
429 in the pontine nuclei (**Figure 7C-E**) or following tracer injection in the head area of M1, in the
430 medial part of the central core of the pontine nuclei (**Figure 7K**). By contrast, tracer injections
431 into S1 areas gave rise to labelled axonal clusters located centrally and caudally in the pontine
432 nuclei (**Figure 7F-J**).

433 In all *Nex-cKO* mice receiving tracer injections into cortical motor areas, the overall
434 distribution of corticopontine labeling (red point clouds in **Figure 7**) was found to be
435 essentially like that observed in the control cases (**Figure 7C-E**). By contrast, tracer injections
436 into S1 representations of the whiskers or upper limb, or into the S1/M1 (sensorimotor) lower
437 limb representation in *Nex-cKO* brains gave rise to abnormal distribution of corticopontine
438 fibers (**Figure 7F-I)**. Specifically, while the S1 corticopontine projections in wild-type mice
439 typically form a large, elongated, caudally or laterally located cluster (**Figure 7F-H**, dark grey
440 points), this labelling was shifted towards more rostral locations in the *Nex-cKO* brains (**Figure**

441 **7F-H**, red points), resembling the distributions observed after tracer injections in motor areas
442 (**Figure 7C-E)**.

443 Notably, tracer injections placed in the anterolateral part of S1 in in *Nex-cKO* mice, in regions
444 representing sensory surfaces of the head, gave rise to labelled axons distributed in the
445 central part of the pontine nuclei, with more subtle difference to the matching control
446 experiments (**Figure 7I)**. In two cases, projections from the S1 head region were distinctly
447 shifted towards medial relative to a control experiments (**Figure 7I, and K**), attaining a
448 distribution resembling the corticopontine projections from head representations in M1
449 cortex, located significantly more anteriorly in the cortex (**Figure 7K**). These results indicate
450 that corticopontine projections from the head representations of S1 also display abnormal
451 topographical distributions resembling the normal projections from homologous
452 representations in the primary motor cortex. Finally, one tracer injection placed in the most
453 anterolateral part of S1, representing perioral surfaces in a *Nex-cKO* mouse, yielded
454 corticopontine labelling which was highly similar to that of a control experiment (**Figure 7J**).

455 Our findings thus show that corticopontine projections from motor areas and the most
456 anterolaterally located parts of S1 are topographically similar in *Nex-cKO* brains and controls,
457 whereas corticopontine projections from most parts of S1 (head, whisker, upper limb, and
458 lower limb representations) are abnormally shifted towards rostral and medial regions of the
459 pontine nuclei, that normally receive projections from cortical motor areas. This is in overall
460 agreement with the spatial and temporal control of Nr2f1 in area mapping. Indeed, no
461 changes in motor-deriving corticopontine projections might be due to low Nr2f1 expression
462 in rostral/motor cortex (spatial control), whereas no changes in the projections originating
463 from the most anterolateral part of S1, the earliest cortical projections to innervate the
464 forming pontine nuclei, might be explained by the late Nr2f1 genetic inactivation occurring
465 after the earliest layer V neurons have been produced (temporal control).

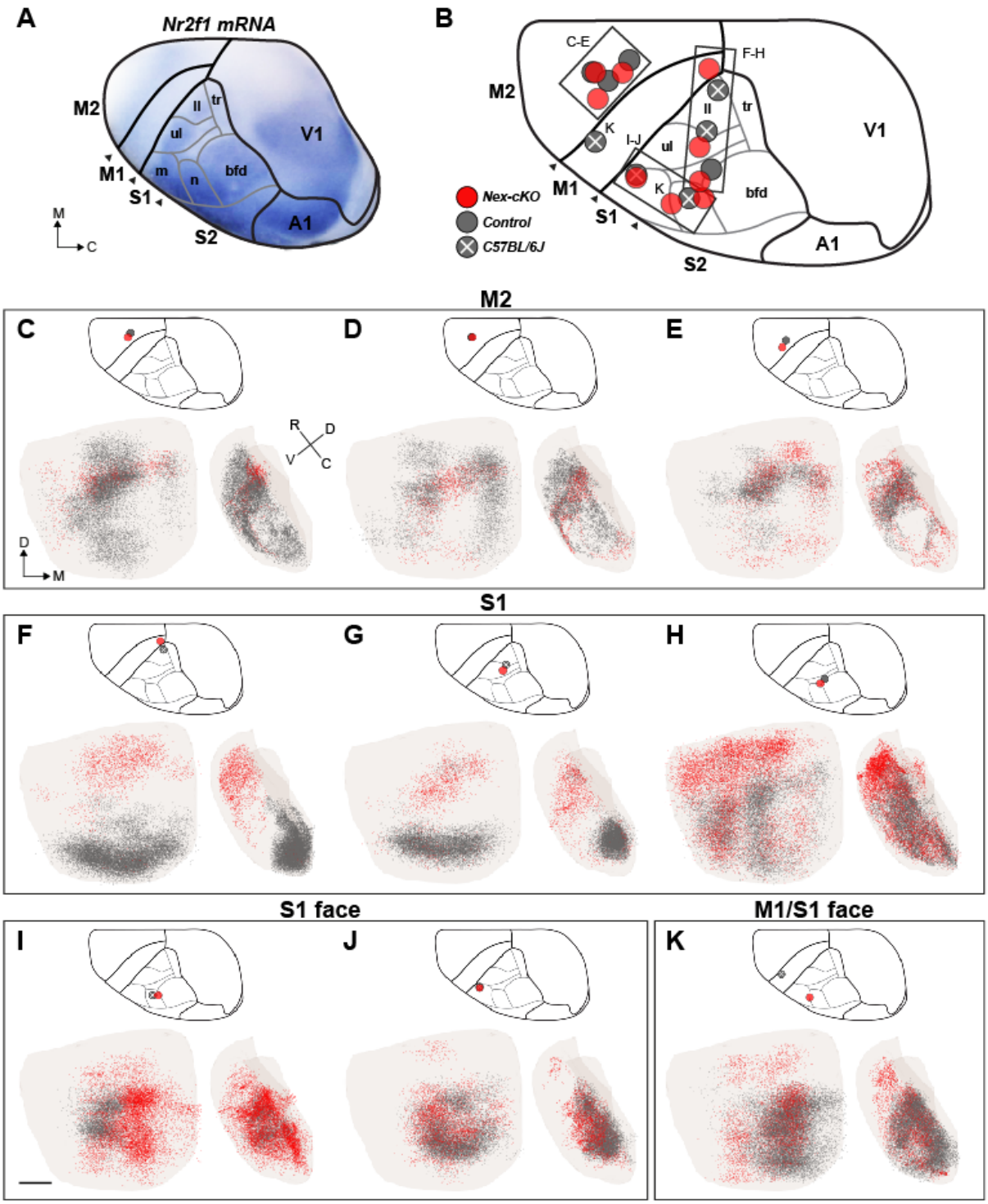

Figure 7. Anterograde tracing of corticopontine projections from motor and somatosensory areas in Nex-cKO mice. *(**A**) Dorsal view of a P5 cortical hemisphere positive for Nr2f1 mRNA transcript, showing graded Nr2f1 expression across the right cerebral cortex, with drawings of cortical area representations transferred from the adult Allen mouse brain atlas. (**B**) Overview of the location of the anterograde viral tracer injection sites in the right primary motor (M1), secondary motor (M2), or primary somatosensory (S1) cortex in Nex-cKO (red), control (dark gray), and wild-type C57BL/6J (dark gray with white cross, data from the Allen Mouse Brain Connectivity Atlas) brains. (**C-J**) 3D colored point clouds representing axonal labeling in corresponding pairs of Nex-cKO (red) or control/wild-type (dark gray) mice, shown within a transparent surface representation of the right pontine nuclei in ventral and medial views. Inset drawings of the brains seen from dorsal show the location of tracer injection sites for each combination of point clouds. Tracer injections in corresponding locations in M2 of both Nex-cKO and control/wild-type mice give rise to quite*

*similar corticopontine labelling in rostrally located clusters, curving towards ventral and caudal along the surface of the pontine nuclei (**C-E**). By contrast, corresponding tracer injections in lower limb and upper limb representing regions in S1 of Nex-cKO and control/wild-type mice give rise to labelling in different parts of the pontine nuclei, with corticopontine projections in control mice distributed in elongated curved clusters located caudally (gray points in **F,G**) or laterally in the pontine nuclei (gray points in **H**), while projections from the same locations in Nex-cKO mice are shifted to more peripheral rostral and lateral parts of the pontine nuclei (red points in **F-H**). All tracer injections in the face region of Nex-cKO and control mice gave rise to labeling in the central region of the pontine nuclei, however with a subtle medial shift of projections in Nex-cKO brains (**I**, see also **K**). Corresponding tracer injections in the most anterolateral part of S1 in a Nex-cKO and wild-type control gave rise to highly similar labeling, centrally in the pontine nuclei. (**K**) Tracer injections in widely separated, homologous locations in S1 (Nex-cKO) and M1 (wild-type control) gave rise to largely corresponding labeling in the medial part of the central core region of the pontine nuclei, albeit with additional rostral and medial labelling in the Nex-cKO experiment. This demonstrates that corticopontine projections from S1 in Nex-cKO mice are changed to resemble normal projections from M2. Abbreviations: A1, primary auditory cortex; bfd, barrel field; C, caudal; D, dorsal; L, lateral; ll, lower limb; M, medial; m, mouth; M1, primary motor cortex; M2, secondary motor cortex; n, nose; PN, pontine nuclei; R, rostral; S1, primary somatosensory cortex; tr, trunk; ul, upper limb. Scale bar, 200 µm.*

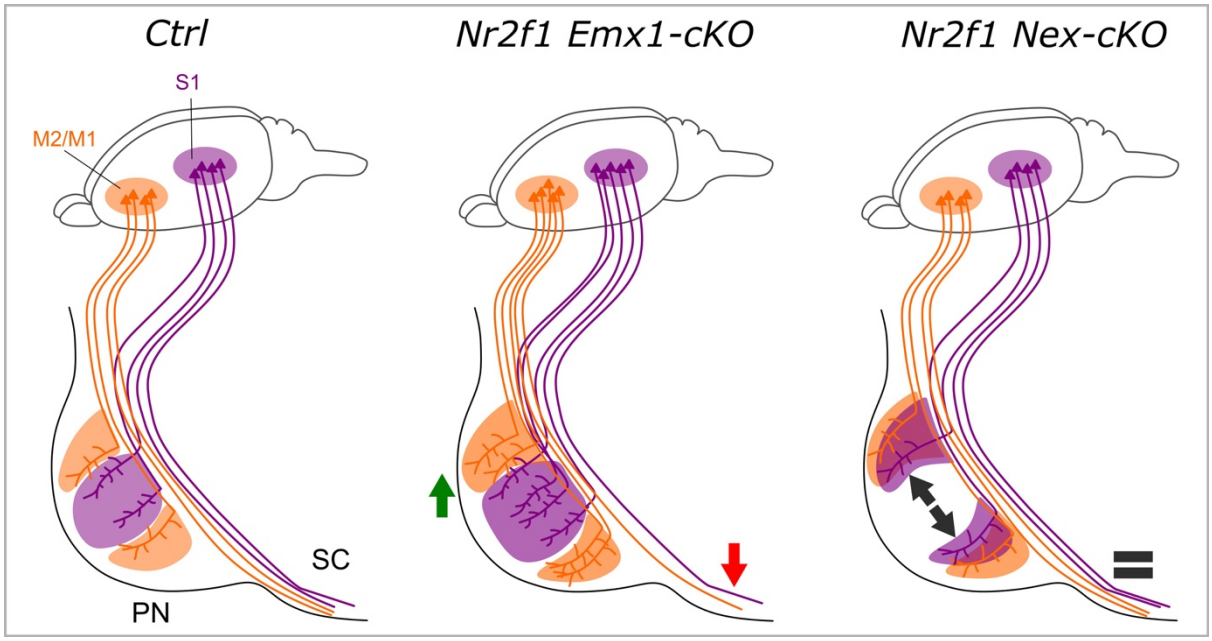

Figure 8. Summary schematics of changes in layer V pyramidal neuron connectivity upon cortical Nr2f1 inactivation. *In control mice (Ctrl), projections from motor areas (M2/M1, orange) and S1 (purple) target largely segregated parts of the pontine nuclei, while a substantial amount of fibers continue towards the spinal cord. Somatosensory projections target the central core region of the PN, while motor projections target more peripheral rostral, caudal, and medial parts of the pontine nuclei. In Nr2f1 Emx1-cKO mutants, in which Nr2f1 expression is lost in cortical progenitors and neurons, fewer fibers reach the SC (red arrow) and more projections target the PN (green arrow), possibly with more diffuse distribution of fibers. In Nr2f1 Nex-cKO animals, in which Nr2f1 expression is inactivated at later stages only in cortical postmitotic neurons, no difference between corticospinal and corticopontine projections are detected (grey equal sign), but corticopontine topography of S1 is affected, whereby fibers reach lateral, motor-receiving PN regions instead of targeting the core (illustrated by grey divergent arrows).*

511 **DISCUSSION**

512 Our present study questions whether and how spatio-temporal cortical expression gradients
513 are involved in the establishment of normal topographical organization of corticopontine
514 projections. By combining genetically modified mice and public mouse brain connectivity
515 data with tract-tracing techniques and digital brain atlas tools, we have provided novel
516 evidence of an intrinsic molecular control of layer V cortical neurons during the establishment
517 of topographical organization of corticopontine projections in a spatial and temporal fashion.
518 Abnormal areal organization in the neocortex induced by Nr2f1 inactivation is reflected in
519 altered corticopontine projections, as well as impaired structural integrity of the CST. While
520 loss of *Nr2f1* from the early progenitor cell pool leads to increased and abnormal
521 corticopontine innervation at the expense of corticospinal projections, only late postmitotic
522 *Nr2f1* inactivation reveals altered topographic pontine mapping from medially located parts
523 of somatosensory cortex controlling whisker, upper limb, and lower limb representations. No
524 shifts from motor and somatosensory anterolateral projections were observed in these mice,
525 in line with a spatial and temporal control of Nr2f1 expression, respectively. Overall, our data
526 show that proper area mapping of the neocortical primordium is a pre-requisite for preserving
527 the cortical spatial and temporal segregation within the pontine nuclei, and thus correct
528 corticopontine topographic organization.

529

530 **Spatial accuracy of topographical data compared across experiments**

531 To ensure proper accuracy of 3D data in wild-type and genetically-modified mice, we relied
532 on spatial alignment of serial microscopic section images to a common atlas reference space,
533 achieved through a two-step atlas registration method (Puchades et al., 2019), which included
534 adjustment of section orientation and non-linear refinement. The process allowed us to
535 record and compare axonal projections as 3D data points in an interactive viewer tool. The
536 use of non-linear registration compensated for minor shape differences among brains and
537 allowed comparison of distribution patterns among spatially relevant data. The focus on the
538 location rather than the amount of signal expression/axonal labelling also compensated for
539 the variation in signal expression intensity and size of tracer injections among cases. The

540 approach to comparing axonal distributions as semi-quantitatively recorded data points in 3D
541 was adopted from well-established methods used in earlier studies of cerebro-cerebellar
542 organization in rats (Leergaard et al., 2000a, Lillehaug et al., 2002, Leergaard and Bjaalie,
543 1995, Leergaard et al., 1995, Leergaard et al., 2000b). By representing signal expression and
544 axonal labeling as 3D point clouds, it became possible to more directly explore and compare
545 location and distribution patterns in 3D in different combinations of data sets. For the
546 additional benchmark data extracted from the *Allen Mouse Brain Connectivity Atlas*, we used
547 the same sagittal image orientation as in our microscopic data, to facilitate comparison of
548 microscopic images in addition to the 3D comparisons. The relevance and accuracy of the
549 approach was confirmed by demonstrating that similarly located cortical tracer injections in
550 control animals gave rise to similarly distributed labelling patterns in the pontine nuclei.

551

552 **Area mapping genes and cortical topography**

553 The cortical primordium is initially pre-specified by the combined action of morphogens
554 secreted by patterning centers that modulate expression gradients of a combination of
555 transcription factors, largely along three orthogonal (anteroposterior, mediolateral and
556 dorsoventral) axes (O'Leary and Nakagawa, 2002, Alfano and Studer, 2012). These
557 transcription factors determine areal fate and regulate expression of downstream molecules
558 that in turn control the topographic organization of synaptic inputs and outputs of related
559 structures (Assimacopoulos et al., 2012, Greig et al., 2013). A new theme of cortical patterning
560 emerges, in which genetic factors intrinsically direct the spatial and temporal establishment
561 of topographically organized axonal connections between the cortex and subcortical brain
562 regions (Cadwell et al., 2019). Our initial hypothesis that cortical patterning genes, such as
563 Nr*2f1*, known to modulate the size and positions of future cortical areas (O'Leary and Sahara,
564 2008, Alfano and Studer, 2012, Cadwell et al., 2019), were good candidates to impart the
565 spatial characteristics of corticopontine projections during development, was also supported
566 by evidence of abnormal specification of layer V neurons upon loss of Nr2f1. For instance, we
567 previously showed (i) abnormal temporal and spatial specification (Alfano et al., 2014,
568 Armentano et al., 2007, Tomassy et al., 2010); (ii) altered intrinsic excitability and dendrite
569 complexity (Del Pino et al., 2020) of layer V neurons in *Nr2f1* cortical mutants, and (iii)

570 behavioral defects in the execution of skilled voluntary movements but not locomotion of
571 adult *Nr2f1* mutant mice (Tomassy et al., 2010). These previous observations prompted us to
572 use Nr2f1 genetic models as a paradigm to hypothesize the implication of cortical area
573 mapping in corticopontine topography.

574

575 **Mitotic versus postmitotic Nr2f1 functions in layer V corticofugal projections**

576 Our previous data showed overall areal organization impairments in both *Nr2f1* mutant
577 brains, independently of whether Nr2f1 was inactivated in progenitors or postmitotic
578 neurons. Then, gain-of-function experiments showed that area identity was most likely due
579 to Nr2f1 expression in postmitotic cells (Alfano et al., 2014). Here, we show for the first time
580 that Nr2f1 drives corticopontine connectivity differently in progenitors *versus* postmitotic
581 neurons. While Nr2f1 expressed by progenitor cells controls the ratio between corticopontine
582 and corticospinal axonal projections, similarly to what happens in *C. elegans* with the ortholog
583 UNC-55 (Zhou and Walthall, 1998, Petersen et al., 2011), postmitotic Nr2f1 expression
584 specifically acts on S1 topographic organization of corticopontine neurons (**Figure 8**). This
585 suggests that early Nr2f1 expression in progenitor cells is mainly required in the specification
586 and axonal guidance of layer V subtypes, while later postmitotic expression is more implicated
587 in the refinement of corticopontine topographical organization. Interestingly, the altered
588 distribution of layer V YFP expression observed in the *Emx1-* and *Nex-cKO* cortex relative to
589 control animals, correspond well with the differences in pontine innervation. A higher
590 production of layer V neurons in S1 of *Emx1-cKO* mice leads to increased corticopontine
591 innervation, in accordance with increased Lmo4 expression, known to drive layer V neurons
592 versus the pontine nuclei (Cederquist et al., 2013, Harb et al., 2016). Differently, the *Nex-cKO*
593 S1 cortex maintains a similar number of YFP layer V neurons, but their axons project to
594 pontine targets normally innervated by motor-derived cortical areas. Since only a
595 subpopulation of layer V neurons express YFP in the S1 barrel field region, as previously
596 reported (Porrero et al., 2010), fewer YFP projections arising from this region are labeled in
597 pontine nuclei, but are nevertheless present, as demonstrated by corticopontine tracer
598 injections from anterolateral cortical regions. Finally, increased signal expression in visual and
599 auditory areas in the occipital cortex, corresponds with an increased innervation in

600 dorsolateral regions of pontine nuclei known to receive projections from the occipital cortex.
601 This observation confirms our main conclusion that postmitotic Nr2f1 expression is involved
602 in determining layer V corticopontine topographical mapping.
603

604 **Revising the chrono-architectonic hypothesis of cortico-pontine circuit development**

605 Previous data in developing rats have shown that pontine neurons settle in the forming
606 pontine nuclei in a shell-like fashion according to their birthdate with early born neurons
607 forming the central core of the pontine nuclei and later born neurons consecutively settling
608 around the earlier born neurons forming concentric rings (Altman and Bayer, 1987). In
609 parallel, at early postnatal stages, corticopontine axons are chemotropically attracted as
610 collateral branches from corticospinal axons (O'Leary and Terashima, 1988, Heffner et al.,
611 1990), and innervate the pontine nuclei in a topographic inside-out pattern (Leergaard et al.,
612 1995), which is further refined through adult stages (Leergaard and Bjaalie, 2007). Neurons in
613 the frontal (motor) cortex project rostrally and medially in the pontine nuclei, neurons in the
614 parietal (somatosensory) cortex project to central and caudal parts, neurons in the temporal
615 (auditory) cortex to central and lateral regions, and neurons in the occipital (visual) cortex to
616 lateral and rostral parts of the pontine nuclei (Leergaard and Bjaalie, 2007). This concentric
617 organization of corticopontine projections suggests that the birthdate of pontine neurons and
618 the inside-out genesis of the pontine nuclei is linked to the spatial organization of cortical
619 inputs.

620 However, intrinsic differences in pontine neurons born at different times might also have an
621 instructive role for corticopontine innervation. A recent study in mice showed that
622 postmitotic expression of the HOX gene *Hoxa5* guides pontine neurons to settle caudally
623 within the pontine nuclei, where they are targeted by projections from limb representations
624 in the somatosensory cortex (Maheshwari et al., 2020). Moreover, ectopic Hoxa5 expression
625 in pontine neurons is sufficient to attract cortical somatosensory inputs, regardless of their
626 spatial position in the pontine nuclei, showing that pontine neurons can play an instructive
627 and attractive role in topographic input connectivity of corticopontine neurons (Maheshwari
628 et al., 2020).

629 Nevertheless, maturational gradients in the pontine nuclei cannot fully explain the complexity
630 of the fine-grained somatotopic topographic connectivity pattern between cortical input and
631 pontine neuron targets. Since the establishment of topographic maps requires multiple
632 processes and structures, it is conceivable that the position and specific intrinsic molecular
633 programs of both presynaptic afferents and postsynaptic target neurons contribute to this
634 complex corticopontine connectivity map. Indeed, our data show that without affecting the
635 development and maturation of pontine neurons, corticopontine Nr2f1-deficient layer V
636 axons originating from S1 areas in the parietal cortex will abnormally target the pontine
637 region normally deputed to corticopontine motor axons. By contrast, Nr2f1-deficient axons
638 originating from the frontal and medial cortex will innervate the expected pontine region
639 allocated to motor axons (**Figure 8**). This strongly suggests that during the establishment of
640 corticopontine topography, both structures, the neocortex and the pons need to be properly
641 pre-patterned by factors involved in spatial and temporal control of neurogenesis, such as
642 Nr2f1 for the cortex, and Hoxa5 for the pontine nuclei.

643

644 **Conclusion and outlook**

645 With the present study, we have provided new insights into the developmental mechanisms
646 establishing topographical organization by showing that gradient cortical expressions of
647 transcription factors, in this case Nr2f1, are directly involved in the establishment of
648 corticopontine topographic mapping. However, it is likely that other factors regulating area
649 size and positions might also be implicated in the same process. We conclude that distinct
650 molecular mechanisms in the source (cerebral cortex) and target (pontine nuclei) regions
651 must be coordinated during the establishment of corticopontine topography. Identifying the
652 molecular pathways within the cortex and pontine nuclei, as well as the mechanisms and
653 molecules governing their interaction remains an open question for further studies.

654

655

656

657 **STAR Methods**

658 **Topographical map of corticopontine projections from somatosensory and motor areas**

659 To establish a 3D benchmark map of corticopontine projections from somatosensory and
660 motor areas in in adult wild type mice, we utilized a selection of public experimental tract-
661 tracing data available from the Allen Institute mouse brain connectivity atlas
662 (http://connectivity.brain-map.org/). We selected 11 experiments in which the anterograde
663 tracer EGFP was injected in the right primary/secondary motor cortex (n =6) or primary
664 somatosensory cortex (n = 5) of wild type C57BL/6J mice (**Supplementary Table 1**). Serial two
665 photon fluorescence images were interactively inspected online using the Projection High
666 Resolution Image viewer of the Allen Institute, and from each case, 5 sagittal oriented images
667 of the right pontine nuclei (matching the orientation of the histological material generated
668 from our knock-out mice), spaced at ~100 μm were captured by screen shot from the largest
669 3D multiplane thumbnail viewer. The resolution of the captured images was up-sampled
670 three times original size before their spatial alignment to the CCFv3 was optimized using the
671 tools QuickNII (Puchades et al., 2019) and VisuAlign (RRID), as described below. These images
672 were used to create 3D representations of the axonal labeling in the pontine nuclei (**Figure 2**;
673 see below).

674 **Animals**

675 All mice used were bred in a C57BL/6J background. Male and female animals at any stage of
676 development were used. All experiments were conducted in accordance with the French
677 Animal Welfare Act and European guidelines for the use of experimental animals, using
678 protocols approved by the French Ministry of Education, Research and Innovation and the
679 local ethics committee (CIEPAL NCE/2019–548, Nice) under authorization #15 349 and #15
680 350. *Nr2f1/COUP-TFI*$^{fl/fl}$ mice were crossed with *Emx1-Cre-recombinase* mice to inactivate
681 *Nr2f1/COUP-TFI* exclusively in cortical progenitors and their progeny (Armentano et al., 2007)
682 or with *Nex-Cre-recombinase* mice to abolish *Nr2f1/COUP-TFI* expression from postmitotic
683 neurons (Alfano et al., 2014). Littermate *Nr2f1/COUP-TFI*$^{fl/fl}$ mice without the presence of the
684 *Cre-recombinase* gene (*Cre-negatives*) were considered controls (**Supplementary Table 2**).
685 For postnatal (P)21 and adult topographic map analysis, *Emx1-cKO* and *Nex-cKO* animals were

686 further crossed with *Thy1-eYFP-H* mice to specifically label layer V projection neurons, as
687 previously reported (Harb et al., 2016, Porrero et al., 2010). Mice were genotyped as
688 previously described (Alfano et al., 2014, Armentano et al., 2007, Harb et al., 2016). Control
689 and mutant littermates were genotyped as *Nr2f1*$^{fl/fl}$*:Thy1-eYFP-H*$^{T/+}$ and *Nr2f1*$^{fl/fl}$*:Emx1-*
690 *Cre:Thy1-eYFP-H*$^{T/+}$ or *Nr2f1*$^{fl/fl}$*:Nex-Cre:Thy1-eYFP-H*$^{T/+}$, respectively. For simplicity, mutant
691 mice are named *Emx1-cKO* and *Nex-cKO* throughout the text. Midday of the day of the
692 observed vaginal plug was considered as embryonic day 0.5 (E0.5).

693 **Anterograde tracing of corticospinal axons in early postnatal mice**

694 P4-P5 animals were anesthetized on ice for 5 min and kept on ice during the whole procedure.
695 Viral particles were produced from the AAV9-CAGtdTomato plasmid by the Alexis Bemelmans
696 (CEA, France) Company, and diluted 1:50 in TE-Buffer (Qiagen, #1018499) to a final
697 concentration of 1.75e12 vg/ml (kindly donated by I. Dusart, Pierre and Marie Curie
698 University, Paris, France). Approximately 0.5/1ul was injected unilaterally in different rostral-
699 caudal and medio-lateral brain locations of control and *Nex-cKO* pups, as previously described
700 in (Gu et al. 2017).

701 **Microscopic imaging**

702 Mosaic microscopic images were acquired using an Axio Imager M2 epifluorescence
703 microscope (Carl Zeiss Microscopy GmbH, Jena, Germany) equipped with a halogen lamp, a
704 MCU 2008 motorized stage, and an EC Plan-Neofluar 10x/0.30 and an AxioCam MRm camera.
705 ZEN blue software was used for imaging and automatic stitching. Images were exported in
706 TIFF format and serially ordered from lateral to medial, rotated and if needed, mirrored to
707 consistent anatomical orientation using Adobe Photoshop CS6 (RRID: SCR_014199), before
708 being converted to PNG format and resized to 60% of original size using ImageJ
709 (RRID:SCR_003070) with bilinear interpolation. The resized serial images were loaded into
710 Adobe Photoshop as a stack, spatially aligned using the ventral surfaces of the pons and
711 cerebral peduncle as landmarks, cropped and exported as individual PNG files.

712 For comparative analyses of topographical organization (see below), variations in YFP signal
713 expression intensity within and between groups were normalized by adjusting the brightness

714 and contrast of images to equal levels using a custom-made histogram matching script
715 available for ImageJ (National Institutes of Health; https://imagej.nih.gov/). One selected,
716 representative case (Experiment 5, Cre-negative, nr: 14250, **Supplementary Table 2**) was
717 used as reference.

718 **Spatial alignment to common 3D reference atlas**

719 Serial sectional images were spatially registered to the *Allen Mouse Common Coordinate*
720 *Framework*, version 3, 2017 edition of the delineations (CCFv3, (Wang et al., 2020) using the
721 QuickNII software tool (RRID:SCR_016854; (Puchades et al., 2019). Multiple anatomical
722 landmarks (hippocampus, caudoputamen, inferior and superior colliculus, and external
723 surface of the neocortex) were used to determine the mediolateral position and orientation
724 of the sagittal section images. For each section image, custom atlas diagrams were aligned to
725 anatomical landmarks in the experimental images using affine transformations, with
726 emphasis on matching the ventral surface of the pons and white matter tracts close to the
727 pontine nuclei and exported as PNG images. To co-display images and the spatially registered
728 custom atlas images, we used the software tool LocaliZoom, which is embedded in the
729 Navigator3 image management system (bit.ly/navigator3), developed and hosted by the
730 Neural Systems Laboratory at the University of Oslo, Norway.

731 **Cortical distribution analysis in *Emx1-cKO* and *Nex-cKO* mutants**

732 Serial section images from *Nex-cKO* and *Emx1-cKO* mutants co-registered to the *Allen Mouse*
733 *Brain Connectivity Atlas* were semi-quantitatively analyzed using a 5-stage scoring table based
734 on relative density of cells in the cortical mantle (**Figure 4A-D')**. Each brain region was scored
735 from 0 (absent signal) to 4 (very high signal), characterized by high number of cells, dense and
736 extensive overlap and intense signal intensity (**Figure 4E)**. The quantifications were
737 summarized graphically and displayed as histograms **(Figure 4F**).

738 **Corticospinal tract morphometric analysis in *Emx1-cKO* and *Nex-cKO* mutants**

739 Serial section images from *Nex-cKO* and *Emx1-cKO* mutants were analyzed by using the *Fiji-*
740 *ImageJ Software* tool (Schindelin et al., 2015) used to determine the total dorsoventral width
741 of the bundle expressing fluorescent signal in the descending fiber tract in different positions:

742 rostrally and caudally to the pontine nuclei, and 250 µm and 500 µm caudal to the nuclei. The
743 width of separate fiber fascicles was also measured 250 µm and 500µm from the terminal
744 edge of the pontine nuclei (**Figure 5A'**).

745 **Analysis of tracer injection sites**

746 Serial section images of cortical tracer injections in *Nex-cKO* brains (**Supplementary Table 3**)
747 and experiments taken from the *Allen Mouse Brain Connectivity Atlas*, were spatially aligned
748 using QuickNII and VisuAlign, as described above. The center positions of the injection sites
749 were annotated as a point-coordinate using LocaliZoom, co-displayed with the CCFv3 atlas in
750 the 3D viewer tool MeshView (RRID:SCR_017222). The mouse brain atlas of Franklin and
751 Paxinos (Franklin and Paxinos, 2008) was used to aid the interpretation of injection site
752 locations. This visualization was used to select spatially corresponding injection site locations
753 for analyses of spatial distribution of corticopontine projections.

754 **Histology, immunohistochemistry and *in situ* hybridization**

755 At age P8, P21 and adulthood, animals were anesthetized by intraperitoneal injection of a
756 mixture of Tiletamine-Zolazepam-Xylazine-Buprenorphine and intracardially perfused with PB
757 Saline (PBS) followed by 4% paraformaldehyde (PFA) in PBS. Volumes were 15, 20 and 30 ml,
758 respectively. Brains were removed from the skull and postfixed for 4 h at 4°C in 4% PFA, before
759 being vibratome-sectioned in 100µm (adult samples) or 150µm (P8 and P21 samples) thick
760 sagittal sections. All sections were incubated overnight at 4°C in a solution of 0.5% Triton X-
761 100, 3% BSA, 10% goat serum in PBS, for permeabilization and reduction of non-specific
762 binding of antibodies. For immunofluorescence (IF), sections were incubated for 2 days at 4°C
763 with primary antibodies in a solution of 0.5% Triton X-100, 10% goat serum in PBS, and then
764 overnight at 4°C with relative secondary antibodies and HOECHST diluted in PBS. For the
765 complete list of primary and secondary antibodies, see **Supplementary Table 5**. Sections were
766 washed several times in PBS, then transferred on Superfrost plus slides (ThermoScientific),
767 covered and dried for 30 min to 1 h, and finally mounted with the Mowiol (Sigma-Aldrich)
768 mounting medium. Whole mount *in situ* hybridization of *Nr2f1 mRNA* on P7 brains was
769 performed according to previously published protocols (Mercurio et al., 2019).

770 **Semi-quantitative recording and 3D visualization of spatial distribution patterns**

771 To investigate and compare the 3D distributions of YFP signal expression or anterograde
772 axonal labelling within the pontine nuclei, we used the annotation functionality in the
773 LocaliZoom tool to semi-quantitatively record YFP signal expression or labelled axons in all
774 sections through the pontine nuclei as point coordinates (specified in the coordinate system
775 of the reference atlas, CCFv3), reflecting the overall density of signal/labelling observed in the
776 images (**Figure 2B,C,G,H)**. To compensate for the spacing between sections and allow
777 inspection of point distributions perpendicularly to the section angle, the z-coordinate of each
778 point was randomly displaced within the thickness of the gap between sections using a
779 custom Python script. The point-coordinates were co-displayed in the MeshView 3D viewer
780 tool (**Figures 2, 3, 6, 7)**.

781 **Data and Code Availability**

782 All microscopic images and derived 3D point coordinate data representing the YFP signal
783 expression or axonal labelling in the pontine nuclei generated in this project will be shared via
784 the EBRAINS research infrastructure (https://search.kg.ebrains.eu/) as high-resolution TIFF
785 images, together with customized, spatially matching reference atlas plates in PNG format.
786 The custom Python script (spread.py) used to randomly displace data points within the
787 thickness of a section is available upon request. The LocaliZoom and Meshview viewer tools
788 are available from https://search.kg.ebrains.eu/

789 **ACKNOWLEDGEMENTS**

790 We thank Isabelle Dusart in Paris for providing us with AAV9-CAG-tdTomato viral particles
791 produced by Alexis Bemelmans (CEA, France), Sara Mercurio and Silvia Nicolis for the Nr2f1
792 stained whole-mount brain, Nicolaas Groeneboom and Gergely Csucs for expert technical
793 assistance, the iBV PRISM platform for imaging support, and Sharon Yates, and Maja A.
794 Puchades for useful discussions. This work was funded by the "Fondation Recherche
795 Médicale; Equipe FRM 2015" #DEQ20150331750 to M.S.; by an ''Investments for the Future''
796 LabEx SIGNALIFE (grant ANR-11- LABX-0028-01) to M.S., by a PhD contract from Région
797 PACA/Inserm and FRM 4th year PhD for C.T, with additional funding from the European

Union's Horizon 2020 Framework Program for Research and Innovation under the Specific Grant Agreement No. 785907 (Human Brain Project SGA2), Specific Grant Agreement No. 945539 (Human Brain Project SGA3), and The Research Council of Norway under Grant Agreement No. 269774 (INCF Norwegian Node) to JGB and TBL.

Competing interests: The authors declare no financial and non-financial competing interests.

804 **SUPPLEMENTARY FIGURES**

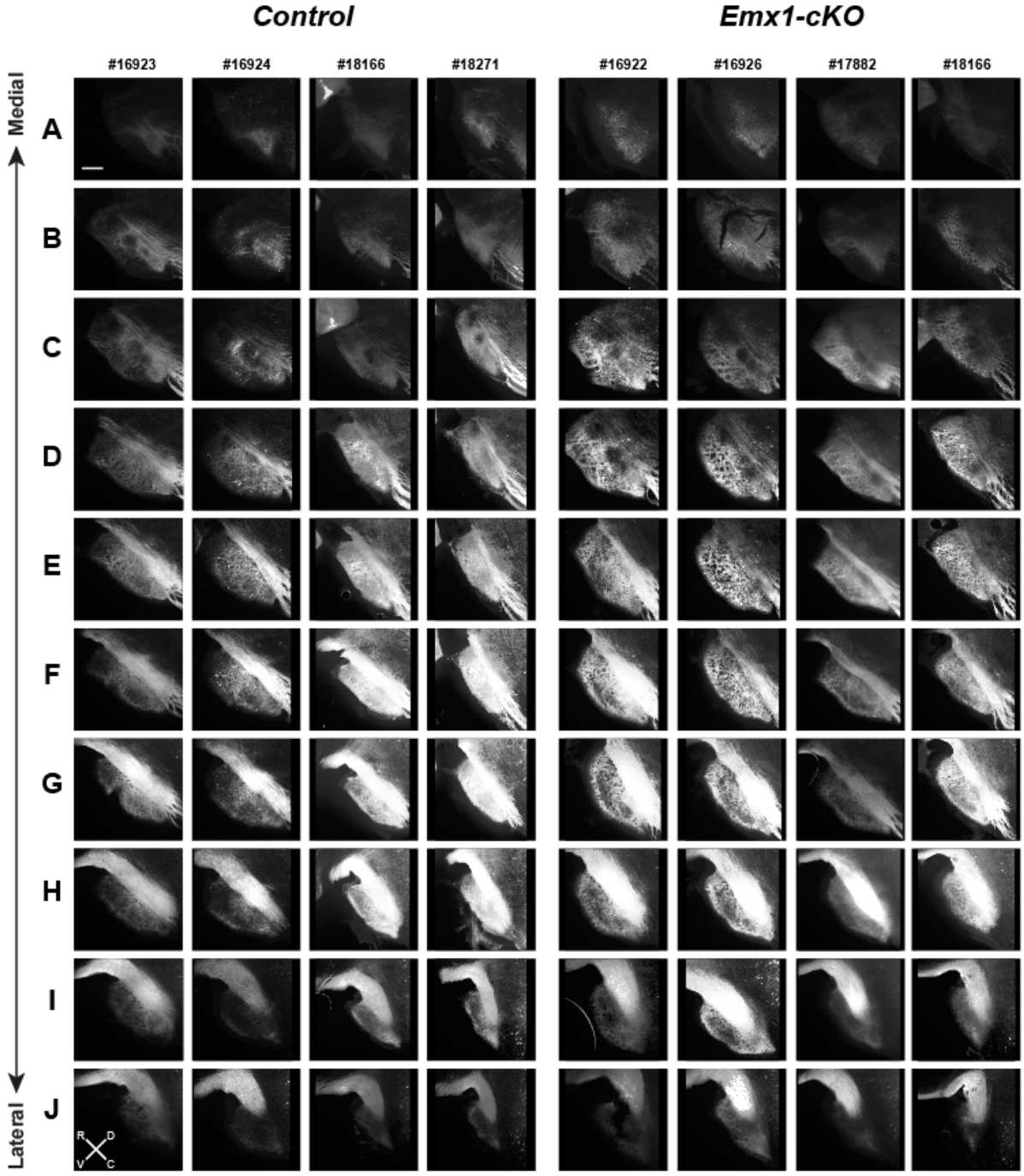

805
806
807 ***Supplementary Figure 1.*** *Fluorescence microscopy images of the pontine nuclei in sagittal sections*
808 *from 4 control- and 4 Emx1-cKO mice. Columns show images from one animal, with sections from*
809 *corresponding levels from medial to lateral are sorted from top to bottom (rows A-J). The intensity*
810 *levels of the images have been normalized. Signal expression in Emx1-cKO mice is more widespread*
811 *and more diffusely distributed in the pontine nuclei, relative to controls. Scale bar, 200 µm.*
812

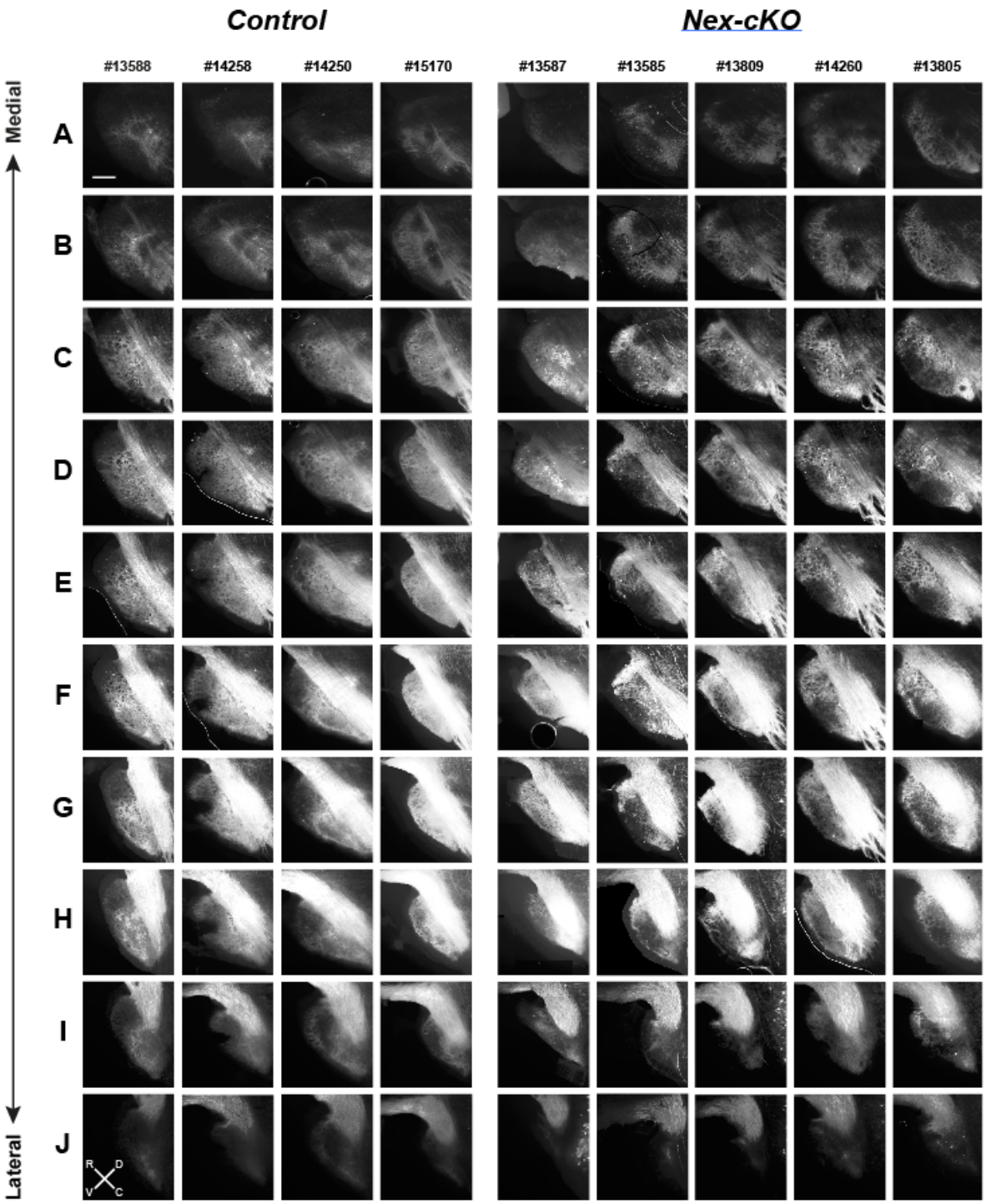

Supplementary Figure 2. *Fluorescence microscopy images of the pontine nuclei in sagittal sections from 4 control- and 4 Nex-cKO mice. Columns show images from one animal, with sections from corresponding levels from medial to lateral are sorted from top to bottom (rows A-J). The intensity levels of the images have been normalized. Signal expression in Nex-cKO mice is more clearly reduced or absent in the central core region of the pontine nuclei, relative to controls. Scale bar, 200 µm.*

821 **SUPPLEMENTARY TABLES**

822 ***Supplementary Table 1***

Allen Mouse Brain Connectivity database					
Experiment number #	**Sex**	**Age (±2)**	**Genotype**	**Injection site**	**Shown in**
100141780	Male	P56	C57BL/6J	Primary motor cortex	Fig. 3, 7B and 7K
114290938	male	P56	C57BL/6J	Primary somatosensory cortex, mouth region	Fig. 2A, 2B, 3, 7B and 7J
112229814	male	P56	C57BL/6J	Primary somatosensory cortex, upper limb region	Fig. 3, 7B and 7F
112952510	male	P56	C57BL/6J	Secondary motor cortex	Fig. 3
114292355	male	P56	C57BL/6J	Primary somatosensory cortex, lower limb region	Fig. 3, 7B and 7F
126908007	male	P56	C57BL/6J	Primary somatosensory cortex, nose region	Fig. 3, 7B and 7I
127084296	male	P56	C57BL/6J	Secondary motor cortex	Fig. 3
127866392	male	P56	C57BL/6J	Primary somatosensory cortex, barrel field region	Fig. 3
141602484	male	P56	C57BL/6J	Secondary motor cortex	Fig. 3
141603190	male	P56	C57BL/6J	Secondary motor cortex	Fig. 3
585025284	male	P56	C57BL/6J	Secondary motor cortex	Fig. 3

823

824 ***Supplementary Table 2***

Adult					
Exp. #	**Animal #**	**Sex**	**Age**	**Genotype**	**Shown in**
1	13588	female	P33	*Thy1-eYFP$^{T/+}$; Nr2f1$^{fl/fl}$*	Fig. 4, 5, 6 and Suppl. Fig.1, 2
1	13587	female	P33	*Thy1-eYFP$^{T/+}$; Nr2f1$^{/fl}$; Nex-Cre*	Fig. 4, 5, 6 and Suppl. Fig.1, 2
2	13585	male	P62	*Thy1-eYFP$^{T/+}$; Nr2f1$^{/fl}$; Nex-Cre*	Fig. 4, 5, 6 and Suppl. Fig.1, 2
3	13809	male	P57	*Thy1-eYFP$^{T/+}$; Nr2f1$^{/fl}$; Nex-Cre*	Fig. 4, 5, 6 and Suppl. Fig.1, 2
4	14258	male	P57	*Thy1-eYFP$^{T/+}$; Nr2f1$^{/fl}$*	Fig. 4, 5, 6 and Suppl. Fig.1, 2
4	14260	male	P57	*Thy1-eYFP$^{T/+}$; Nr2f1$^{/fl}$; Nex-Cre*	Fig. 4, 5, 6 and Suppl. Fig.1, 2
5	13805	male	P55	*Thy1-eYFP$^{T/+}$; Nr2f1$^{/fl}$; Nex-Cre*	Fig. 4, 5, 6 and Suppl. Fig.1, 2
5	14250	male	P72	*Thy1-eYFP$^{T/+}$; Nr2f1$^{/fl}$*	Fig. 4, 5, 6 and Suppl. Fig.1, 2
5	15170	male	P75	*Thy1-eYFP$^{T/+}$; Nr2f1$^{/fl}$*	Fig. 4, 5, 6 and Suppl. Fig.1, 2
6	16922	male	P76	*Thy1-eYFP$^{T/+}$; Nr2f1$^{/fl}$; Emx1-Cre*	Fig. 4, 5, 6 and Suppl. Fig.1, 2
6	16923	male	P76	*Thy1-eYFP$^{T/+}$; Nr2f1$^{/fl}$*	Fig. 4, 5, 6 and Suppl. Fig.1, 2
6	16924	male	P76	*Thy1-eYFP$^{T/+}$; Nr2f1$^{/fl}$*	Fig. 4, 5, 6 and Suppl. Fig.1, 2
6	16926	male	P76	*Thy1-eYFP$^{T/+}$; Nr2f1$^{/fl}$; Emx1-Cre*	Fig. 4, 5, 6 and Suppl. Fig.1, 2
7	17882	male	P72	*Thy1-eYFP$^{T/+}$; Nr2f1$^{/fl}$; Emx1-Cre*	Fig. 4, 5, 6 and Suppl. Fig.1, 2
8	18046	female	P109	*Thy1-eYFP$^{T/+}$; Nr2f1$^{/fl}$; Emx1-Cre*	Fig. 4, 5, 6 and Suppl. Fig.1, 2
8	18166	female	P98	*Thy1-eYFP$^{T/+}$; Nr2f1$^{/fl}$*	Fig. 4, 5, 6 and Suppl. Fig.1, 2
8	18271	female	P87	*Thy1-eYFP$^{T/+}$; Nr2f1$^{/fl}$*	Fig. 4, 5, 6 and Suppl. Fig.1, 2
9	19606	female	P86	*Thy1-eYFP$^{T/+}$; Nr2f1$^{/fl}$; Emx1-Cre*	Fig. 5
9	19607	female	P86	*Thy1-eYFP$^{T/+}$; Nr2f1$^{/fl}$; Emx1-Cre*	Fig. 5

825

826 ***Supplementary Table 3***

P21 – unilateral CST tracing			
Tracer injected in motor cortex			
Experiment #	**Animal #**	**Genotype**	**Shown in**
2	11643_13	*Ctrl*	Fig. 7B and 7C
2	11643_16	*Nex-cKO*	Not shown
2	11643_17	*Nex-cKO*	Fig. 7B and 7E
2	11796_2	*Ctrl*	Not shown
2	11796_8	*Ctrl*	Not shown
2	11796_9	*Ctrl*	Not shown
3	18035_1	*Ctrl*	Fig. 7B and 7E
3	18035_2	*Ctrl*	Fig. 7B and 7D
3	18035_7	*Ctrl*	Not shown
3	18035_3	*Nex-cKO*	Fig. 7B and 7D
3	18035_4	*Nex-cKO*	Not shown
3	18035_8	*Nex-cKO*	Fig. 7B and 7C
4	19423_2	*Ctrl*	Not shown
4	19423_3	*Ctrl*	Not shown
4	19423_4	*Nex-cKO*	Not shown
4	19423_5	*Nex-cKO*	Not shown
Tracer injected in somatosensory cortex			
4	19423_6	*Nex-cKO*	Fig. 7B and 7F
4	19423_7	*Nex-cKO*	Fig. 7B and 7G
6	11431_1	*Nex-cKO*	Fig. 7B and 7I
6	11431_3	*Nex-cKO*	Fig. 7B and 7H
6	11431_4	*Nex-cKO*	Fig. 7B and 7K
6	11431_6	*Ctrl*	Fig. 7B and 7H
6	11431_7	*Nex-cKO*	Fig. 2F, 2G, 7B and 7J

827
828
829

830 ***Supplementary Table 4:***

831

Figure 4 – Cortical distribution of YFP-H positive cells

Area	Hypothesis	Mean 1	Mean 2	Mean diff.	95,00% CI of diff	Summary	Adjusted P.
PFC	*Ctrl vs. Nex-cKO*	1.172	0.3174	0.8543	-0.209 to 1.918	ns	0.3142
	Ctrl vs. Emx1-cKO	1.172	0.9523	0.2194	-0.8439 to 1.283	ns	>0.9999
	Nex-cKO vs. Emx1-cKO	0.3174	0.9523	-0.6349	-1.8 to 0.5299	ns	>0.9999
ACC	*Ctrl vs. Nex-cKO*	2.411	1.104	1.307	0.2434 to 2.37	**	0.0042
	Ctrl vs. Emx1-cKO	2.411	1.411	1	-0.06316 to 2.063	ns	0.0897
	Nex-cKO vs. Emx1-cKO	1.104	1.411	-0.3065	-1.471 to 0.8583	ns	>0.9999
GC	*Ctrl vs. Nex-cKO*	0.5317	0.09524	0.4365	-0.7283 to 1.601	****	<0.0001
	Ctrl vs. Emx1-cKO	0.5317	0.09524	0.4365	-0.7283 to 1.601	ns	0.1008
	Nex-cKO vs. Emx1-cKO	0.09524	0.09524	0	-1.345 to 1.345	***	0.0001
M2	*Ctrl vs. Nex-cKO*	1.515	2.773	1.515	1.709 to 3.836	****	<0.0001
	Ctrl vs. Emx1-cKO	3.301	0.9872	3.301	-0.07613 to 2.051	ns	>0.9999
	Nex-cKO vs. Emx1-cKO	3.301	-1.785	3.301	-2.95 to -0.6207	****	<0.0001
M1	*Ctrl vs. Nex-cKO*	4.217	1.818	2.399	1.336 to 3.462	ns	>0.9999
	Ctrl vs. Emx1-cKO	4.217	3.703	0.5139	-0.5495 to 1.577	**	0.0016
	Nex-cKO vs. Emx1-cKO	1.818	3.703	-1.885	-3.05 to -0.7202	****	<0.0001
S1	*Ctrl vs. Nex-cKO*	3.346	2.922	0.4237	-0.6396 to 1.487	ns	>0.9999
	Ctrl vs. Emx1-cKO	3.346	4.74	-1.394	-2.458 to -0.331	**	0.0016
	Nex-cKO vs. Emx1-cKO	2.922	4.74	-1.818	-2.983 to -0.6533	****	<0.0001
A	*Ctrl vs. Nex-cKO*	0.8868	1.803	-0.9158	-1.979 to 0.1475	ns	0.1883
	Ctrl vs. Emx1-cKO	0.8868	3.66	-2.773	-3.836 to -1.71	****	<0.0001
	Nex-cKO vs. Emx1-cKO	1.803	3.66	-1.857	-3.022 to -0.6922	****	<0.0001
V	*Ctrl vs. Nex-cKO*	0.9544	2.686	-1.732	-2.795 to -0.6684	****	<0.0001
	Ctrl vs. Emx1-cKO	0.9544	4.045	-3.091	-4.154 to -2.027	****	<0.0001
	Nex-cKO vs. Emx1-cKO	2.686	4.045	-1.359	-2.524 to -0.1942	**	0.0086
RSC	*Ctrl vs. Nex-cKO*	0.8826	2.101	-1.219	-2.282 to -0.1553	*	0.0108
	Ctrl vs. Emx1-cKO	0.8826	3.024	-2.142	-3.205 to -1.078	****	<0.0001
	Nex-cKO vs. Emx1-cKO	2.101	3.024	-0.923	-2.088 to 0.2418	ns	0.3454

Figure 5E – Rostral LFP diameter

Section	Hypothesis	Mean 1	Mean 2	Mean diff.	95,00% CI of diff	Summary	Adjusted P.
1	*Ctrl vs. Nex-cKO*	0	0	0	-116.9 to 116.9	ns	>0.9999
	Ctrl vs. Emx1-cKO	0	0	0	-116.9 to 116.9	ns	>0.9999
	Nex-cKO vs. Emx1-cKO	0	0	0	-124.9 to 124.9	ns	>0.9999
2	*Ctrl vs. Nex-cKO*	0	28.29	-28.29	-145.2 to 88.57	ns	0.836
	Ctrl vs. Emx1-cKO	0	0	0	-116.9 to 116.9	ns	>0.9999
	Nex-cKO vs. Emx1-cKO	28.29	0	28.29	-96.64 to 153.2	ns	0.8549
3	*Ctrl vs. Nex-cKO*	0	132.7	-132.7	-249.6 to -15.84	*	0.0215
	Ctrl vs. Emx1-cKO	0	0	0	-116.9 to 116.9	ns	>0.9999
	Nex-cKO vs. Emx1-cKO	132.7	0	132.7	7.775 to 257.6	*	0.0343
4	*Ctrl vs. Nex-cKO*	0	179.6	-179.6	-296.5 to -62.77	**	0.001
	Ctrl vs. Emx1-cKO	0	0	0	-116.9 to 116.9	ns	>0.9999
	Nex-cKO vs. Emx1-cKO	179.6	0	179.6	54.71 to 304.6	**	0.0023
5	*Ctrl vs. Nex-cKO*	0	175.9	-175.9	-292.8 to -59.04	**	0.0013
	Ctrl vs. Emx1-cKO	0	55.34	-55.34	-172.2 to 61.52	ns	0.5052
	Nex-cKO vs. Emx1-cKO	175.9	55.34	120.6	-4.369 to 245.5	ns	0.0612
6	*Ctrl vs. Nex-cKO*	24.35	169.6	-145.2	-262.1 to -28.37	*	0.0103
	Ctrl vs. Emx1-cKO	24.35	115	-90.67	-207.5 to 26.2	ns	0.1624
	Nex-cKO vs. Emx1-cKO	169.6	115	54.57	-70.37 to 179.5	ns	0.5592
7	*Ctrl vs. Nex-cKO*	117	231.4	-114.4	-231.3 to 2.467	ns	0.0565
	Ctrl vs. Emx1-cKO	117	234.6	-117.7	-234.5 to -0.8201	*	0.048
	Nex-cKO vs. Emx1-cKO	231.4	234.6	-3.287	-128.2 to 121.6	ns	0.9979
8	*Ctrl vs. Nex-cKO*	241.7	187.5	54.13	-66.26 to 174.5	ns	0.5401
	Ctrl vs. Emx1-cKO	241.7	293	-51.33	-171.7 to 69.06	ns	0.5746
	Nex-cKO vs. Emx1-cKO	187.5	293	-105.5	-230.4 to 19.47	ns	0.1168
9	*Ctrl vs. Nex-cKO*	316.6	267.9	48.71	-68.15 to 165.6	ns	0.5888
	Ctrl vs. Emx1-cKO	316.6	250.1	66.55	-56.81 to 189.9	ns	0.4128
	Nex-cKO vs. Emx1-cKO	267.9	250.1	17.83	-113.2 to 148.9	ns	0.9449
10	*Ctrl vs. Nex-cKO*	318.9	194.4	124.6	7.715 to 241.4	*	0.0335
	Ctrl vs. Emx1-cKO	318.9	205.8	113.1	-3.738 to 230	ns	0.0602
	Nex-cKO vs. Emx1-cKO	194.4	205.8	-11.45	-136.4 to 113.5	ns	0.9746
11	*Ctrl vs. Nex-cKO*	231.1	88.06	143.1	-163 to 449.1	ns	0.514
	Ctrl vs. Emx1-cKO	231.1	64.04	167.1	-82.79 to 416.9	ns	0.258
	Nex-cKO vs. Emx1-cKO	88.06	64.04	24.02	-225.8 to 273.9	ns	0.9721

12	*Ctrl vs. Nex-cKO*	276.1	179.6	96.5	-26.86 to 219.9	ns	0.1576
	Ctrl vs. Emx1-cKO	276.1	136.5	139.6	16.23 to 263	*	0.022
	Nex-cKO vs. Emx1-cKO	179.6	136.5	43.09	-93.77 to 179.9	ns	0.7389
13	*Ctrl vs. Nex-cKO*	201.9	180.5	21.33	-243.7 to 286.3	ns	0.9804
	Ctrl vs. Emx1-cKO	201.9	44.45	157.4	-40.14 to 354.9	ns	0.1471
	Nex-cKO vs. Emx1-cKO	180.5	44.45	136.1	-113.8 to 385.9	ns	0.4059
14	*Ctrl vs. Nex-cKO*	218.4	114.6	103.8	-19.52 to 227.2	ns	0.1182
	Ctrl vs. Emx1-cKO	218.4	95.41	123	-0.3344 to 246.4	ns	0.0508
	Nex-cKO vs. Emx1-cKO	114.6	95.41	19.19	-117.7 to 156	ns	0.9416
15	*Ctrl vs. Nex-cKO*	154.7	59.11	95.61	-21.25 to 212.5	ns	0.1328
	Ctrl vs. Emx1-cKO	154.7	51.17	103.6	-13.31 to 220.4	ns	0.0942
	Nex-cKO vs. Emx1-cKO	59.11	51.17	7.94	-117 to 132.9	ns	0.9877
16	*Ctrl vs. Nex-cKO*	101.6	16.85	84.78	-32.09 to 201.6	ns	0.2035
	Ctrl vs. Emx1-cKO	101.6	18.75	82.87	-33.99 to 199.7	ns	0.2183
	Nex-cKO vs. Emx1-cKO	16.85	18.75	-1.908	-126.8 to 123	ns	0.9993
17	*Ctrl vs. Nex-cKO*	60.94	0	60.94	-55.93 to 177.8	ns	0.4374
	Ctrl vs. Emx1-cKO	60.94	0	60.94	-55.93 to 177.8	ns	0.4374
	Nex-cKO vs. Emx1-cKO	0	0	0	-124.9 to 124.9	ns	>0.9999
18	*Ctrl vs. Nex-cKO*	28.85	0	28.85	-88.02 to 145.7	ns	0.8301
	Ctrl vs. Emx1-cKO	28.85	0	28.85	-88.02 to 145.7	ns	0.8301
	Nex-cKO vs. Emx1-cKO	0	0	0	-124.9 to 124.9	ns	>0.9999
19	*Ctrl vs. Nex-cKO*	0	0	0	-112 to 112	ns	>0.9999
	Ctrl vs. Emx1-cKO	0	0	0	-116.9 to 116.9	ns	>0.9999
	Nex-cKO vs. Emx1-cKO	0	0	0	-120.4 to 120.4	ns	>0.9999

Figure 5F – Caudal LFP diameter

Section	Hypothesis	Mean 1	Mean 2	Mean diff.	95,00% CI of diff	Summary	Adjusted P.
1	*Ctrl vs. Nex-cKO*	0	0	0	-88.51 to 88.51	ns	>0.9999
	Ctrl vs. Emx1-cKO	0	0	0	-88.51 to 88.51	ns	>0.9999
	Nex-cKO vs. Emx1-cKO	0	0	0	-94.62 to 94.62	ns	>0.9999
2	*Ctrl vs. Nex-cKO*	0	46.89	-46.89	-135.4 to 41.62	ns	0.4252
	Ctrl vs. Emx1-cKO	0	0	0	-88.51 to 88.51	ns	>0.9999
	Nex-cKO vs. Emx1-cKO	46.89	0	46.89	-47.73 to 141.5	ns	0.4728
3	*Ctrl vs. Nex-cKO*	0	98.1	-98.1	-186.6 to -9.584	*	0.0257
	Ctrl vs. Emx1-cKO	0	0	0	-88.51 to 88.51	ns	>0.9999
	Nex-cKO vs. Emx1-cKO	98.1	0	98.1	3.473 to 192.7	*	0.0402
4	*Ctrl vs. Nex-cKO*	0	126.2	-126.2	-214.7 to -37.72	**	0.0026
	Ctrl vs. Emx1-cKO	0	0	0	-88.51 to 88.51	ns	>0.9999
	Nex-cKO vs. Emx1-cKO	126.2	0	126.2	31.6 to 220.9	**	0.0053
5	*Ctrl vs. Nex-cKO*	18.5	111	-92.51	-181 to -3.999	*	0.0382
	Ctrl vs. Emx1-cKO	18.5	13.31	5.196	-83.32 to 93.71	ns	0.9895
	Nex-cKO vs. Emx1-cKO	111	13.31	97.71	3.084 to 192.3	*	0.0412
6	*Ctrl vs. Nex-cKO*	69.28	128.1	-58.82	-147.3 to 29.69	ns	0.2617
	Ctrl vs. Emx1-cKO	69.28	97.47	-28.19	-116.7 to 60.32	ns	0.7331
	Nex-cKO vs. Emx1-cKO	128.1	97.47	30.63	-63.99 to 125.3	ns	0.7256
7	*Ctrl vs. Nex-cKO*	107.5	176	-68.56	-300.3 to 163.2	ns	0.765
	Ctrl vs. Emx1-cKO	107.5	152.1	-44.66	-227.9 to 138.6	ns	0.8336
	Nex-cKO vs. Emx1-cKO	176	152.1	23.9	-159.3 to 207.1	ns	0.9491
8	*Ctrl vs. Nex-cKO*	175.2	237.2	-61.95	-157.9 to 34.02	ns	0.2821
	Ctrl vs. Emx1-cKO	175.2	154.5	20.69	-70.49 to 111.9	ns	0.8541
	Nex-cKO vs. Emx1-cKO	237.2	154.5	82.63	-16.61 to 181.9	ns	0.1235
9	*Ctrl vs. Nex-cKO*	214.5	138.2	76.34	-12.17 to 164.9	ns	0.1063
	Ctrl vs. Emx1-cKO	214.5	197.7	16.82	-71.69 to 105.3	ns	0.8952
	Nex-cKO vs. Emx1-cKO	138.2	197.7	-59.52	-154.1 to 35.1	ns	0.3005
10	*Ctrl vs. Nex-cKO*	209.6	115.1	94.49	5.983 to 183	*	0.0333
	Ctrl vs. Emx1-cKO	209.6	132	77.6	-10.91 to 166.1	ns	0.0988
	Nex-cKO vs. Emx1-cKO	115.1	132	-16.89	-111.5 to 77.73	ns	0.9069
11	*Ctrl vs. Nex-cKO*	232.5	99.13	133.4	44.9 to 221.9	**	0.0013
	Ctrl vs. Emx1-cKO	232.5	116.2	116.4	27.87 to 204.9	**	0.0061
	Nex-cKO vs. Emx1-cKO	99.13	116.2	-17.03	-111.7 to 77.59	ns	0.9055
12	*Ctrl vs. Nex-cKO*	186.4	127.8	58.65	-34.78 to 152.1	ns	0.302
	Ctrl vs. Emx1-cKO	186.4	26.38	160.1	71.56 to 248.6	****	<0.0001
	Nex-cKO vs. Emx1-cKO	127.8	26.38	101.4	2.179 to 200.7	*	0.0439
13	*Ctrl vs. Nex-cKO*	94.47	0	94.47	-137.3 to 326.2	ns	0.6019
	Ctrl vs. Emx1-cKO	94.47	13.38	81.09	-95.93 to 258.1	ns	0.527
	Nex-cKO vs. Emx1-cKO	0	13.38	-13.38	-190.4 to 163.6	ns	0.9826

14	*Ctrl vs. Nex-cKO*	58.1	0	58.1	-33.08 to 149.3	ns	0.2913
	Ctrl vs. Emx1-cKO	58.1	0	58.1	-33.08 to 149.3	ns	0.2913
	Nex-cKO vs. Emx1-cKO	0	0	0	-94.62 to 94.62	ns	>0.9999
15	*Ctrl vs. Nex-cKO*	0	0	0	-84.82 to 84.82	ns	>0.9999
	Ctrl vs. Emx1-cKO	0	0	0	-88.51 to 88.51	ns	>0.9999
	Nex-cKO vs. Emx1-cKO	0	0	0	-91.18 to 91.18	ns	>0.9999
Figure 5G – Rostral LFP area							
	Hypothesis	**Mean 1**	**Mean 2**	**Mean diff.**	**95,00% CI of diff**	**Summary**	**Adjusted P.**
	Ctrl vs. Nex-cKO	2414	2258	156.4	-570.3 to 883	ns	0.8257
	Ctrl vs. Emx1-cKO	2414	1725	689.2	-37.42 to 1416	ns	0.0637
Figure 5H – Caudal LFP area							
	Hypothesis	**Mean 1**	**Mean 2**	**Mean diff.**	**95,00% CI of diff**	**Summary**	**Adjusted P.**
	Ctrl vs. Nex-cKO	1403	1427	-24.29	-261.8 to 213.2	ns	0.9566
	Ctrl vs. Emx1-cKO	1403	884.1	518.8	281.3 to 756.3	***	0.0001
Figure 5I – Fasciculation Index							
Region	**Hypothesis**	**Mean 1**	**Mean 2**	**Mean diff.**	**95,00% CI of diff**	**Summary**	**Adjusted P.**
250 μm	*Ctrl vs. Nex-cKO*	0.6528	0.5493	0.1035	0.01185 to 0.1951	*	0.0216
	Ctrl vs. Emx1-cKO	0.6528	0.5595	0.09326	0.001658 to 0.1849	*	0.0446
500 μm	*Ctrl vs. Nex-cKO*	0.674	0.5771	0.0969	0.00254 to 0.1913	*	0.0422
	Ctrl vs. Emx1-cKO	0.674	0.5146	0.1594	0.06502 to 0.2537	***	0.0004

Summary of statistical analysis and results. *Highlighted in blue, comparisons that produced statistically significant P-values. P-values are calculated by 2way ANOVA test (**Figures 4F and 5E-F**), or ordinary one-way ANOVA test (**Figures 5G-I**).*

Supplementary Table 5: List of primary and secondary antibodies used in this study.

Antigen	Provider	Catalog #	Species	Working dilution
GFP	Abcam	Ab13970	Ck	1:500
RFP	Abcam	Ab 124754	Rb	1:500
Ck IgY - AF 488	Thermo Fisher	A11039	Gt	1:500
Rb IgG - AF 555	Thermo Fisher	A21428	Gt	1:500

840 **REFERENCES:**

841 Alfano, C., Magrinelli, E., Harb, K., Hevner, R. F. and Studer, M. (2014) 'Postmitotic control of
842 sensory area specification during neocortical development', *Nat Commun,* 5, pp.
843 5632.
844 Alfano, C. and Studer, M. (2012) 'Neocortical arealization: Evolution, mechanisms and open
845 questions', *Dev Neurobiol*.
846 Altman, J. and Bayer, S. A. (1987) 'Development of the precerebellar nuclei in the rat: IV. The
847 anterior precerebellar extramural migratory stream and the nucleus reticularis
848 tegmenti pontis and the basal pontine gray', *J Comp Neurol,* 257(4), pp. 529-52.
849 Altman J, Bayer SA (1996) Development of the cerebellar system in relation to its evolution,
850 structure and functions. CRC Press,Boca Raton
851 Armentano, M., Chou, S. J., Tomassy, G. S., Leingartner, A., O'Leary, D. D. and Studer, M.
852 (2007) 'COUP-TFI regulates the balance of cortical patterning between frontal/motor
853 and sensory areas', *Nat Neurosci,* 10(10), pp. 1277-86.
854 Assimacopoulos, S., Kao, T., Issa, N. P. and Grove, E. A. (2012) 'Fibroblast growth factor 8
855 organizes the neocortical area map and regulates sensory map topography', *J*
856 *Neurosci,* 32(21), pp. 7191-201.
857 Badura, A., Schonewille, M., Voges, K., Galliano, E., Renier, N., Gao, Z., Witter, L., Hoebeek,
858 F. E., Chedotal, A. and De Zeeuw, C. I. (2013) 'Climbing fiber input shapes reciprocity
859 of Purkinje cell firing', *Neuron,* 78(4), pp. 700-13.
860 Bertacchi, M., Parisot, J. and Studer, M. (2019) 'The pleiotropic transcriptional regulator
861 COUP-TFI plays multiple roles in neural development and disease', *Brain Res,* 1705,
862 pp. 75-94.
863 Bjaalie, J. G. and Brodal, P. (1989) 'Visual pathways to the cerebellum: segregation in the
864 pontine nuclei of terminal fields from different visual cortical areas in the cat',
865 *Neuroscience,* 29(1), pp. 95-107.
866 Bjaalie, J. G. and Brodal, P. (1997) 'Cat pontocerebellar network: numerical capacity and
867 axonal collateral branching of neurones in the pontine nuclei projecting to individual
868 paraflocculcular folia', *Neurosci Res,* 27(3), pp. 199-210.
869 Bower, J. M. (2011) 'Functional implications of tactile projection patterns to the lateral
870 hemispheres of the cerebellum of the albino rat: the legacy of Wally Welker', *Ann N*
871 *Y Acad Sci,* 1225, pp. 130-41.
872 Bower, J. M., Beermann, D. H., Gibson, J. M., Shambes, G. M. and Welker, W. (1981)
873 'Principles of organization of a cerebro-cerebellar circuit. Micromapping the
874 projections from cerebral (SI) to cerebellar (granule cell layer) tactile areas of rats',
875 *Brain Behav Evol,* 18(1-2), pp. 1-18.
876 Bower, J. M. and Kassel, J. (1990) 'Variability in tactile projection patterns to cerebellar folia
877 crus IIA of the Norway rat', *J Comp Neurol,* 302(4), pp. 768-78.
878 Brodal, P. (1978) 'The corticopontine projection in the rhesus monkey. Origin and principles
879 of organization', *Brain,* 101(2), pp. 251-83.
880 Brodal, P. and Bjaalie, J. G. (1992) 'Organization of the pontine nuclei', *Neurosci Res,* 13(2),
881 pp. 83-118.
882 Buckner, R. L. (2013) 'The cerebellum and cognitive function: 25 years of insight from
883 anatomy and neuroimaging', *Neuron,* 80(3), pp. 807-15.
884 Cadwell, C. R., Bhaduri, A., Mostajo-Radji, M. A., Keefe, M. G. and Nowakowski, T. J. (2019)
885 'Development and Arealization of the Cerebral Cortex', *Neuron,* 103(6), pp. 980-
886 1004.

887 Cederquist, G. Y., Azim, E., Shnider, S. J., Padmanabhan, H. and Macklis, J. D. (2013) 'Lmo4
888 establishes rostral motor cortex projection neuron subtype diversity', *J Neurosci,*
889 33(15), pp. 6321-32.
890 Chapin, J. K. and Lin, C. S. (1984) 'Mapping the body representation in the SI cortex of
891 anesthetized and awake rats', *J Comp Neurol,* 229(2), pp. 199-213.
892 D'Elia, K. P. and Dasen, J. S. (2018) 'Topographic Maps: Motor Axons Wait Their Turn', *Curr*
893 *Biol,* 28(2), pp. R86-R88.
894 Del Pino, I., Tocco, C., Magrinelli, E., Marcantoni, A., Ferraguto, C., Tomagra, G., Bertacchi,
895 M., Alfano, C., Leinekugel, X., Frick, A. and Studer, M. (2020) 'COUP-TFI/Nr2f1
896 Orchestrates Intrinsic Neuronal Activity during Development of the Somatosensory
897 Cortex', *Cereb Cortex,* 30(11), pp. 5667-5685.
898 Erzurumlu, R. S., Murakami, Y. and Rijli, F. M. (2010) 'Mapping the face in the
899 somatosensory brainstem', *Nat Rev Neurosci,* 11(4), pp. 252-63.
900 Fabri, M. and Burton, H. (1991) 'Ipsilateral cortical connections of primary somatic sensory
901 cortex in rats', *J Comp Neurol,* 311(3), pp. 405-24.
902 Feng, G., Mellor, R. H., Bernstein, M., Keller-Peck, C., Nguyen, Q. T., Wallace, M., Nerbonne,
903 J. M., Lichtman, J. W. and Sanes, J. R. (2000) 'Imaging neuronal subsets in transgenic
904 mice expressing multiple spectral variants of GFP', *Neuron,* 28(1), pp. 41-51.
905 Flore, G., Di Ruberto, G., Parisot, J., Sannino, S., Russo, F., Illingworth, E. A., Studer, M. and
906 De Leonibus, E. (2017) 'Gradient COUP-TFI Expression Is Required for Functional
907 Organization of the Hippocampal Septo-Temporal Longitudinal Axis', *Cereb Cortex,*
908 27(2), pp. 1629-1643.
909 Fritzsch, B., Elliott, K. L. and Pavlinkova, G. (2019) 'Primary sensory map formations reflect
910 unique needs and molecular cues specific to each sensory system', *F1000Res,* 8.
911 Goebbels, S., Bormuth, I., Bode, U., Hermanson, O., Schwab, M. H. and Nave, K. A. (2006)
912 'Genetic targeting of principal neurons in neocortex and hippocampus of NEX-Cre
913 mice', *Genesis,* 44(12), pp. 611-21.
914 Greig, L. C., Woodworth, M. B., Galazo, M. J., Padmanabhan, H. and Macklis, J. D. (2013)
915 'Molecular logic of neocortical projection neuron specification, development and
916 diversity', *Nat Rev Neurosci,* 14(11), pp. 755-69.
917 Harb, K., Magrinelli, E., Nicolas, C. S., Lukianets, N., Frangeul, L., Pietri, M., Sun, T., Sandoz,
918 G., Grammont, F., Jabaudon, D., Studer, M. and Alfano, C. (2016) 'Area-specific
919 development of distinct projection neuron subclasses is regulated by postnatal
920 epigenetic modifications', *Elife,* 5.
921 Heffner, C. D., Lumsden, A. G. and O'Leary, D. D. (1990) 'Target control of collateral
922 extension and directional axon growth in the mammalian brain', *Science,* 247(4939),
923 pp. 217-20.
924 Henschke, J. U. and Pakan, J. M. (2020) 'Disynaptic cerebrocerebellar pathways originating
925 from multiple functionally distinct cortical areas', *Elife,* 9.
926 Inoue, K., Terashima, T. and Inoue, Y. (1991) 'Postnatal development of the pontine
927 projections from the visual cortex of the mouse', *Okajimas Folia Anat Jpn,* 67(6), pp.
928 479-92.
929 Leergaard, T. B. (2003) 'Clustered and laminar topographic patterns in rat cerebro-pontine
930 pathways', *Anat Embryol (Berl),* 206(3), pp. 149-62.
931 Leergaard, T. B., Alloway, K. D., Mutic, J. J. and Bjaalie, J. G. (2000a) 'Three-dimensional
932 topography of corticopontine projections from rat barrel cortex: correlations with
933 corticostriatal organization', *J Neurosci,* 20(22), pp. 8474-84.

Leergaard, T. B., Alloway, K. D., Pham, T. A., Bolstad, I., Hoffer, Z. S., Pettersen, C. and Bjaalie, J. G. (2004) 'Three-dimensional topography of corticopontine projections from rat sensorimotor cortex: comparisons with corticostriatal projections reveal diverse integrative organization', *J Comp Neurol,* 478(3), pp. 306-22.

Leergaard, T. B. and Bjaalie, J. G. (1995) 'Semi-automatic data acquisition for quantitative neuroanatomy. MicroTrace--computer programme for recording of the spatial distribution of neuronal populations', *Neurosci Res,* 22(2), pp. 231-43.

Leergaard, T. B. and Bjaalie, J. G. (2007) 'Topography of the complete corticopontine projection: from experiments to principal Maps', *Front Neurosci,* 1(1), pp. 211-23.

Leergaard, T. B., Lakke, E. A. and Bjaalie, J. G. (1995) 'Topographical organization in the early postnatal corticopontine projection: a carbocyanine dye and 3-D computer reconstruction study in the rat', *J Comp Neurol,* 361(1), pp. 77-94.

Leergaard, T. B., Lillehaug, S., De Schutter, E., Bower, J. M. and Bjaalie, J. G. (2006) 'Topographical organization of pathways from somatosensory cortex through the pontine nuclei to tactile regions of the rat cerebellar hemispheres', *Eur J Neurosci,* 24(10), pp. 2801-12.

Leergaard, T. B., Lyngstad, K. A., Thompson, J. H., Taeymans, S., Vos, B. P., De Schutter, E., Bower, J. M. and Bjaalie, J. G. (2000b) 'Rat somatosensory cerebropontocerebellar pathways: spatial relationships of the somatotopic map of the primary somatosensory cortex are preserved in a three-dimensional clustered pontine map', *J Comp Neurol,* 422(2), pp. 246-66.

Lemon, R. N. (2008) 'Descending pathways in motor control', *Annu Rev Neurosci,* 31, pp. 195-218.

Lillehaug, S., Oyan, D., Leergaard, T. B. and Bjaalie, J. G. (2002) 'Comparison of semi-automatic and automatic data acquisition methods for studying three-dimensional distributions of large neuronal populations and axonal plexuses', *Network,* 13(3), pp. 343-56.

Liu, Q., Dwyer, N. D. and O'Leary, D. D. (2000) 'Differential expression of COUP-TFI, CHL1, and two novel genes in developing neocortex identified by differential display PCR', *J Neurosci,* 20(20), pp. 7682-90.

Maheshwari, U., Kraus, D., Vilain, N., Holwerda, S. J. B., Cankovic, V., Maiorano, N. A., Kohler, H., Satoh, D., Sigrist, M., Arber, S., Kratochwil, C. F., Di Meglio, T., Ducret, S. and Rijli, F. M. (2020) 'Postmitotic Hoxa5 Expression Specifies Pontine Neuron Positional Identity and Input Connectivity of Cortical Afferent Subsets', *Cell Rep,* 31(11), pp. 107767.

McLaughlin, T. and O'Leary, D. D. (2005) 'Molecular gradients and development of retinotopic maps', *Annu Rev Neurosci,* 28, pp. 327-55.

Mercurio, S., Serra, L., Motta, A., Gesuita, L., Sanchez-Arrones, L., Inverardi, F., Foglio, B., Barone, C., Kaimakis, P., Martynoga, B., Ottolenghi, S., Studer, M., Guillemot, F., Frassoni, C., Bovolenta, P. and Nicolis, S. K. (2019) 'Sox2 Acts in Thalamic Neurons to Control the Development of Retina-Thalamus-Cortex Connectivity', *iScience,* 15, pp. 257-273.

Mihailoff, G. A., Lee, H., Watt, C. B. and Yates, R. (1985) 'Projections to the basilar pontine nuclei from face sensory and motor regions of the cerebral cortex in the rat', *J Comp Neurol,* 237(2), pp. 251-63.

Mottolese, C., Richard, N., Harquel, S., Szathmari, A., Sirigu, A. and Desmurget, M. (2013) 'Mapping motor representations in the human cerebellum', *Brain,* 136(Pt 1), pp. 330-42.

Nitschke, M. F., Kleinschmidt, A., Wessel, K. and Frahm, J. (1996) 'Somatotopic motor representation in the human anterior cerebellum. A high-resolution functional MRI study', *Brain,* 119 (Pt 3), pp. 1023-9.

O'Leary, D. D. and Nakagawa, Y. (2002) 'Patterning centers, regulatory genes and extrinsic mechanisms controlling arealization of the neocortex', *Curr Opin Neurobiol,* 12(1), pp. 14-25.

O'Leary, D. D. and Sahara, S. (2008) 'Genetic regulation of arealization of the neocortex', *Curr Opin Neurobiol,* 18(1), pp. 90-100.

O'Leary, D. D. and Terashima, T. (1988) 'Cortical axons branch to multiple subcortical targets by interstitial axon budding: implications for target recognition and "waiting periods"', *Neuron,* 1(10), pp. 901-10.

Peterburs, J. and Desmond, J. E. (2016) 'The role of the human cerebellum in performance monitoring', *Curr Opin Neurobiol,* 40, pp. 38-44.

Petersen, S. C., Watson, J. D., Richmond, J. E., Sarov, M., Walthall, W. W. and Miller, D. M., 3rd (2011) 'A transcriptional program promotes remodeling of GABAergic synapses in Caenorhabditis elegans', *J Neurosci,* 31(43), pp. 15362-75.

Polleux, F., Dehay, C. and Kennedy, H. (1997) 'The timetable of laminar neurogenesis contributes to the specification of cortical areas in mouse isocortex', *J Comp Neurol,* 385(1), pp. 95-116.

Porrero, C., Rubio-Garrido, P., Avendano, C. and Clasca, F. (2010) 'Mapping of fluorescent protein-expressing neurons and axon pathways in adult and developing Thy1-eYFP-H transgenic mice', *Brain Res,* 1345, pp. 59-72.

Pourchet, O., Morel, M. P., Welniarz, Q., Sarrazin, N., Marti, F., Heck, N., Gallea, C., Doulazmi, M., Roig Puiggros, S., Moreno-Bravo, J. A., Vidailhet, M., Trembleau, A., Faure, P., Chedotal, A., Roze, E. and Dusart, I. (2021) 'Loss of floor plate Netrin-1 impairs midline crossing of corticospinal axons and leads to mirror movements', *Cell Rep,* 34(3), pp. 108654.

Proville, R. D., Spolidoro, M., Guyon, N., Dugue, G. P., Selimi, F., Isope, P., Popa, D. and Lena, C. (2014) 'Cerebellum involvement in cortical sensorimotor circuits for the control of voluntary movements', *Nat Neurosci,* 17(9), pp. 1233-9.

Puchades, M. A., Csucs, G., Ledergerber, D., Leergaard, T. B. and Bjaalie, J. G. (2019) 'Spatial registration of serial microscopic brain images to three-dimensional reference atlases with the QuickNII tool', *PLoS One,* 14(5), pp. e0216796.

Schindelin, J., Rueden, C. T., Hiner, M. C. and Eliceiri, K. W. (2015) 'The ImageJ ecosystem: An open platform for biomedical image analysis', *Mol Reprod Dev,* 82(7-8), pp. 518-29.

Schmahmann, J. D. and Pandya, D. N. (1997) 'Anatomic organization of the basilar pontine projections from prefrontal cortices in rhesus monkey', *J Neurosci,* 17(1), pp. 438-58.

Shambes, G. M., Gibson, J. M. and Welker, W. (1978) 'Fractured somatotopy in granule cell tactile areas of rat cerebellar hemispheres revealed by micromapping', *Brain Behav Evol,* 15(2), pp. 94-140.

Shepherd, G. M. (2009) 'Intracortical cartography in an agranular area', *Front Neurosci,* 3(3), pp. 337-43.

Smart, I. H. (1984) 'Histogenesis of the mesocortical area of the mouse telencephalon', *J Anat,* 138 (Pt 3), pp. 537-52.

1026 Stoodley, C. J. and Schmahmann, J. D. (2010) 'Evidence for topographic organization in the
1027 cerebellum of motor control versus cognitive and affective processing', *Cortex,* 46(7),
1028 pp. 831-44.
1029 Tomasch, J. (1968) 'The overall information carrying capacity of the major afferent and
1030 efferent cerebellar cell and fiber systems', *Confin Neurol,* 30(5), pp. 359-67.
1031 Tomasch, J. (1969) '[The renal pelvis of the dromedary]', *Z Anat Entwicklungsgesch,* 128(3),
1032 pp. 235-42.
1033 Tomassy, G. S., De Leonibus, E., Jabaudon, D., Lodato, S., Alfano, C., Mele, A., Macklis, J. D.
1034 and Studer, M. (2010) 'Area-specific temporal control of corticospinal motor neuron
1035 differentiation by COUP-TFI', *Proc Natl Acad Sci U S A,* 107(8), pp. 3576-81.
1036 Wang, Q., Ding, S. L., Li, Y., Royall, J., Feng, D., Lesnar, P., Graddis, N., Naeemi, M., Facer, B.,
1037 Ho, A., Dolbeare, T., Blanchard, B., Dee, N., Wakeman, W., Hirokawa, K. E., Szafer, A.,
1038 Sunkin, S. M., Oh, S. W., Bernard, A., Phillips, J. W., Hawrylycz, M., Koch, C., Zeng, H.,
1039 Harris, J. A. and Ng, L. (2020) 'The Allen Mouse Brain Common Coordinate
1040 Framework: A 3D Reference Atlas', *Cell,* 181(4), pp. 936-953 e20.
1041 Welker, C. (1971) 'Microelectrode delineation of fine grain somatotopic organization of
1042 (SmI) cerebral neocortex in albino rat', *Brain Res,* 26(2), pp. 259-75.
1043 Woolsey, T. A. and Van der Loos, H. (1970) 'The structural organization of layer IV in the
1044 somatosensory region (SI) of mouse cerebral cortex. The description of a cortical
1045 field composed of discrete cytoarchitectonic units', *Brain Res,* 17(2), pp. 205-42.
1046 Zhou, C., Tsai, S. Y. and Tsai, M. J. (2001) 'COUP-TFI: an intrinsic factor for early
1047 regionalization of the neocortex', *Genes Dev,* 15(16), pp. 2054-9.
1048 Zhou, H. M. and Walthall, W. W. (1998) 'UNC-55, an orphan nuclear hormone receptor,
1049 orchestrates synaptic specificity among two classes of motor neurons in
1050 Caenorhabditis elegans', *J Neurosci,* 18(24), pp. 10438-44.
1051